



## Research paper

# Multi-objective optimization framework for deepwater riser jetting installation parameters using deep reinforcement learning

Yu Song<sup>a,\*</sup>, Zehua Song<sup>a</sup>, Jin Yang<sup>b</sup>, Lei Li<sup>b</sup><sup>a</sup> College of Information Science and Engineering/College of Artificial Intelligence, China University of Petroleum (Beijing), Beijing 102249, China<sup>b</sup> College of Safety and Ocean Engineering, China University of Petroleum (Beijing), Beijing 102249, China

## ARTICLE INFO

## Keywords:

Conductor casing jetting  
Deep reinforcement learning  
Composite action-value Q-learning  
Operational efficiency  
Markov decision process

## ABSTRACT

Optimizing conductor casing installation in offshore oil and gas exploration is essential for underwater wellhead reliability. Traditional models often struggle with the complexities of this process, characterized by jetting drilling and soaking phases. To address this issue, a novel approach using deep reinforcement learning is introduced for comprehensive optimization of jetting parameters, enhancing deep-sea drilling efficiency. The methodology begins with an orthogonal simulated experiment to compile a robust dataset. Following pre-processing, including feature extraction and parameter scaling, a predictive model is developed to correlate installation parameters with jetting and soaking time. A composite action-value Q-learning (CAPQL) based multi-objective reinforcement learning framework is employed, establishing a Markov decision process environment for simultaneous optimization of jetting time and soaking periods. Applying this framework to selected deep-sea wells demonstrates a significant decrease in jetting drilling time (average 46.18%) and soaking time (22.57%), with the predictive model achieving a 99.32% average fit. This approach effectively navigates parameter interdependencies, ensuring optimal outcomes across diverse objectives. These findings present a groundbreaking approach for conductor casing jetting, offering greater precision and efficiency in offshore drilling operations and the potential to redefine industry standards.

## 1. Introduction

In deep-sea drilling operations, optimizing the conductor casing jetting installation parameters is crucial (Zhao et al., 2022; Yang, 2023; Wang et al., 2022). The installation process has two phases: the descent phase, which includes the casing insertion time, and soaking time during the stabilization phase (Wang et al., 2022). Together, these phases determine the efficiency and cost-effectiveness of the installation. However, the complex interaction of the jetting parameters in both phases challenges traditional optimization techniques. Thus, accurate optimization of these parameters is a significant challenge in deep-sea drilling (Zhou et al., 2016).

The research history in this domain is extensive. King et al. discussed the design of deep-water casings using riser and pile foundation analysis models; these models were based on several assumptions, including installation conditions and synthesized behaviors such as applied loads. However, the reliability of these models is not always guaranteed, which leads to structural inadequacies in some wells (King and Solomon, 1995). Jeanjean proposed a method for determining the load-bearing

capacity of casings, providing clear guidance for calculating the instantaneous load-bearing potential of the casing and estimating a timeline for soil strength recovery. Although this method has proven effective in the deep waters of the Gulf of Mexico, its worldwide applicability is yet to be confirmed (Jeanjean, 2002). Akers elucidated the design processes and operational practices of jetting installation structures in deep-water environments, analyzed the force equilibrium during casing descent, and proposed a basic calculation for the casing load-bearing capacity and descent depth. However, this empirically-based method tends to be conservative (Akers, 2008). In terms of simulations, Wang et al. used the Herschel–Bulkley model in ANSYS Fluent to model a viscous soil body and applied the VOF method to simulate the descent of the conductor casing during jetting, determining the impact of nozzle placement, jet velocity, and undrained shear strength of the formation on the dimensions of soil erosion induced by the water jet (Wang and Song, 2019). Liu et al. considered the spatial heterogeneity of nozzles in a three-dimensional context, creating a viable model for calculating the drill bit extension (Liu et al., 2022). In studies on soil shear strength, Lee et al. conducted

\* Corresponding author.

E-mail address: [songyu\\_cup@163.com](mailto:songyu_cup@163.com) (Y. Song).

laboratory-controlled experiments with varying ratios of clay minerals to determine the undrained shear strength of formations under different soil conditions (Lee et al., 1999). Beck et al. using rock mechanics and geotechnics, developed real-time equations for vertical load bearing during casing descent suitable for measuring the vertical friction and load bearing of conductor casings during drilling operations (Beck et al., 1991). Wang et al. established a relationship between the undrained shear strength of the soil and the lateral frictional resistance of the casing, showing a linear correlation between the two for various basin soil profiles (Wang and Sun, 2008). Xu et al. explored the impact of the bearing capacity growth factor of subsea soil on the setting depth of conductors in deepwater drilling (Xu et al., 2014).

Despite numerous studies on optimizing the jetting drilling time for conductor casing installation, complexities arise from many intertwined influencing factors. In practice, there are multiple optimization objectives, such as jetting drilling time, soaking time, vertical load bearing of the casing, and lateral loads, which can potentially conflict, making the resolution challenging.

Recently, as an automated decision-optimizing machine learning approach, deep reinforcement learning (DRL) has shown significant breakthroughs in addressing complex decision-making problems (Hribar et al., 2022; Li et al., 2020; Kim et al., 2022). As a result, DRL has become a promising method for effectively optimizing the installation parameters for conductor casing jetting. However, most DRL methodologies focus on single-objective optimization, whereas real-world conductor casing jetting installations require the simultaneous consideration of multiple objectives. To address this gap, this study introduces a multi-objective deep reinforcement learning algorithm based on composite action-value Q-learning (CAPQL) tailored to optimize the conductor casing jetting installation parameters.

Within the CAPQL framework, a sophisticated neural network model is initially constructed to simulate an authentic conductor casing jetting installation process. A reward function was meticulously designed to encapsulate all the optimization objectives. Through this mechanism, the CAPQL algorithm obtains optimization feedback for all objectives from environmental interactions, subsequently recalibrating its decision-making strategy in response. Additionally, a novel training approach was proposed, enabling the CAPQL algorithm to balance diverse optimization objectives and prevent the excessive optimization of one objective at the expense of others. Ultimately, the empirical validation highlighted the efficacy of the CAPQL algorithm in optimizing the duration of conductor casing jetting installation, with the results indicating significant improvements across multiple optimization objectives.

The primary goal of this research is to offer a novel solution to the optimization challenge of conductor casing jetting installation duration. By leveraging the capabilities of multi-objective deep reinforcement learning, this study aims to achieve a balanced optimization across multiple objectives, thereby enhancing the efficiency of conductor casing jetting installations.

## 2. Methodology

**Step 1. Data Acquisition and Preprocessing:** A layered soil model was constructed to simulate the geological environment of the seafloor. Orthogonal experiments were conducted to monitor and document the relevant data during the conductor casing injection installation process. These data include the depth, drilling pressure, flow rate, undrained shear strength of the formation, bit-to-casing size ratio, internal friction angle, and drill bit extension. The undrained shear strength data of the formation underwent one-dimensional signal processing for feature extraction. The z-score method was used for feature scaling and subsequent data processing.

**Step 2. Training of the Fully Connected Neural Network Model:** The preprocessed data were fed into the neural network model to mimic the actual conductor casing injection installation process. The

input parameters consisted of the aforementioned preprocessed metrics, and the output metrics were the jet drilling and soaking times. Particle swarm optimization was used for the initial optimization of the neural network hyperparameters, whereas a grid search was implemented for further fine-tuning.

**Step 3. Implementation of the Multi-Objective Deep Reinforcement Learning Algorithm,** with drilling pressure, flow rate, bit-to-casing size ratio, and drill bit extension as decision variables and jet drilling and soaking time as optimization targets—aimed at deriving Pareto-optimal solutions to achieve a balanced optimization between the jet drilling and soaking time.

**Step 4. Model Deployment and Case Study:** The best-performing multi-objective deep reinforcement learning model was deployed on a server. Subsequently, a case study is conducted in a specific block for validation and in-depth analyses.

Throughout the workflow, the installation time for the conductor casing injection was systematically optimized. The primary objective is to minimize both jet drilling and soaking times, thereby elevating the efficiency and safety of deep-sea drilling operations.

## 3. Simulation experiments and data processing

In the research on optimizing the installation time of a conductor casing using a multi-objective deep reinforcement learning algorithm, the effectiveness of the algorithm is strongly associated with the quality of its sample set. To ensure the performance of the algorithm during the jetting installation of the conductor casing, experiments were conducted to simulate the jetting descent and installation procedures using a jetting apparatus (Kan et al., 2016). Fig. 1 illustrates the experimental systems for simulating the conductor–casing insertion process and load-bearing simulation.

### 3.1. Jetting installation simulation for conductor casing

During the jetting installation simulation, various parameters were set, including drilling pressure, flow rate, drill bit extension, and bit-to-casing size ratio. Detailed records of the drilling and soaking times throughout the installation process were maintained. Given the potential for dynamic adjustment of these variables in real conductor casing jetting scenarios, they were chosen as primary research variables, holding significant practical implications for studying jetting descent and installation processes.

#### 3.1.1. Experimental setup

Multiple representative layered soil models have been designed (Al-Bared and Marto, 2017). Each model incorporates different layers, such as floating mud, soft mud, muddy silty sand, and hard mud (Brevik et al., 2016). To ensure the realism of the stratum simulation, the rainfall method was used to create sand samples similar to those found in shallow regions of the South China Sea. For cohesive soils, shallow beach cohesive soil was selected, and structured soil models were prepared using low-temperature stirring to control interparticle cementation. Parameters such as layer thickness, buoyancy, average moisture content, undrained shear strength of the formation, and internal friction angle were meticulously set to guarantee model accuracy. Notably, both the undrained shear strength of the formation and the internal friction angle were considered in the geotechnical parameters to encompass a range of soil types, including both cohesive and non-cohesive soils. This comprehensive approach allowed for a more accurate simulation of diverse marine geological conditions. Table 1 lists the geotechnical parameters of the representative strata.

Under each soil model condition, comprehensive experiments were conducted using all the variable combinations. Data were extracted to form a complete dataset and explore the effects of variable settings on jetting, drilling, and soaking time.

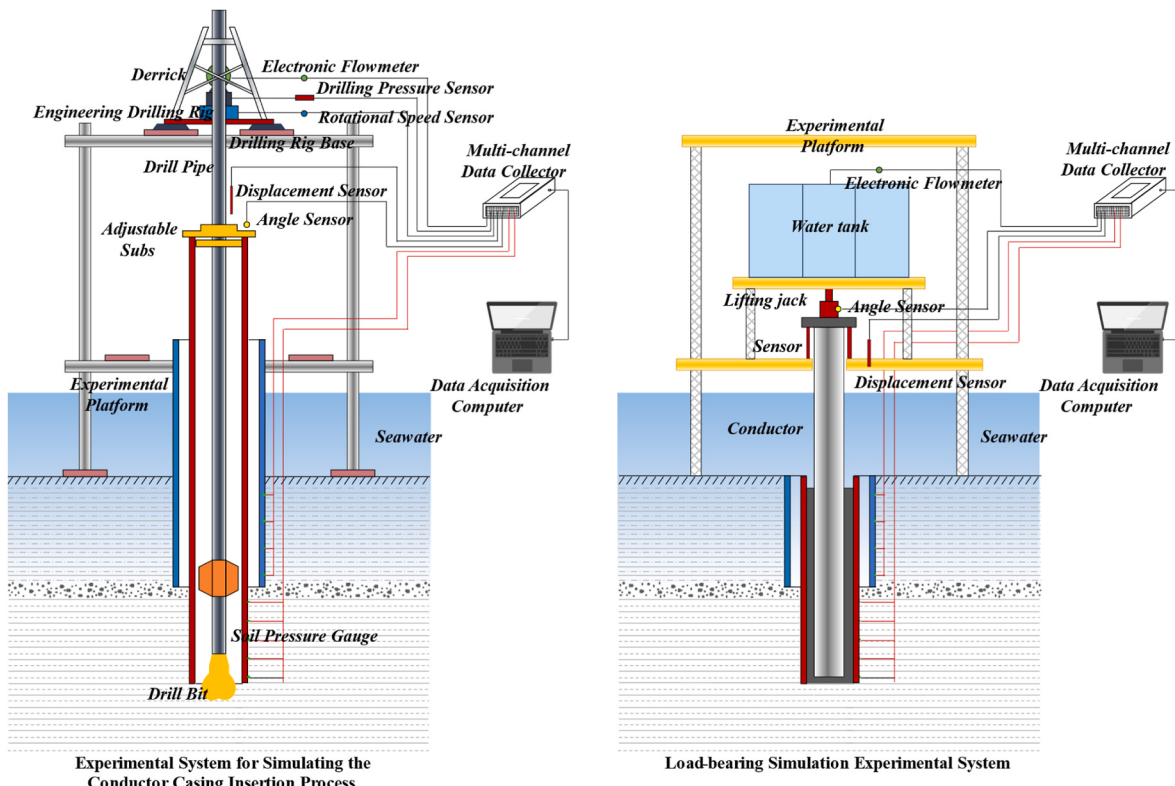


Fig. 1. Structural schematic.

**Table 1**  
Geotechnical parameters of a representative stratum.

Geological Layer	Soil Type	Thickness (m)	Buoyancy (kN/m <sup>3</sup> )	Average Moisture Content (%)	Average Undrained Shear Strength (kPa)	Internal Friction Angle (°)
No.1	Floating Mud Layer	0.2	13.4	92	0	0
No.2	Soft Mud	4.1	16.8	56.2	8.2	32.6
No.3	Muddy Silty Sand	0.4	17.6	54.3	9.9	35.1
No.4	Hard Mud Layer	8.6	19.7	35.9	107.6	42

The detailed design and fabrication of the experimental setup are key to ensuring the accuracy of the experiments. Advanced sensors and instruments were utilized to monitor various parameters during the experimental process, including the depth, drilling pressure, flow rate, drill bit extension, and formation pressure. These data were subjected to intensive analysis after the experiment to identify the specific impacts of each parameter on jetting drilling and soaking time. Moreover, a simulated drill bit, conductor casing, drill rod, and stabilizing joints were manufactured from stainless steel to simulate the properties of the actual drilling equipment. The mud pump design ensured precise control over fluid displacement during the jetting procedure (Changbin et al., 2018).

### 3.1.2. Experimental run components

The design and operation of the simulation components for conductor casing deployment were crucial in this study because they directly influenced the efficiency and outcomes of the jetting installation. The construction of these components involves both the physical properties of the casing (such as length, diameter, and material) and equipment capable of controlling and measuring the jetting parameters.

A simulated conductor casing was fabricated using stainless steel to mirror the material characteristics of actual subsea pipelines. The length and diameter adaptations of the casing were tailored based on the requirements of real-world scenarios. To emulate genuine offshore

operational environments, the casing was designed with adequate rigidity to withstand the pressures imposed by the seabed soil, thus preventing excessive deformation or damage. Specialized jetting apparatuses were integrated within the casing, consisting of a high-pressure pump and an adjustable nozzle. The pump generated ample force for the jet stream, whereas the adjustable nozzle facilitated precision control over the jetting direction and intensity. These design specifications allowed for the replication of the true jetting conditions, enabling an accurate assessment of the impact of various parameters on the jetting installation efficiency during the experiments.

Throughout the experiment, state-of-the-art sensor technologies were employed to monitor and log the parameters in real-time. For example, pressure sensors measure the jetting pressure inside a casing, displacement sensors gauge the descent of the casing, and inclinometers track its inclination. Additionally, the jetting drilling time was acquired by monitoring the speed of casing insertion. The insertion speed, a crucial metric for casing installation efficiency, was analyzed by altering parameters such as drilling fluid discharge, drill bit extension, and bit-to-casing size ratios. These adjustments recorded the casing installation speeds under various soil strength conditions to understand the factors affecting the installation efficiency.

After the experimentation, the soaking time was determined by monitoring soil stress changes around the casing and vertical load-bearing capacity alterations under the designated recovery conditions.

The vertical ultimate load-bearing capacity of the casing is a pivotal parameter for assessing casing-bearing stability. The experimental setups delineated the principal factors affecting the casing load-bearing safety and documented soaking time data.

Key experimental apparatuses included:

**Simulated CADA Tool:** This device connected the simulated casing and drill rod, enabling axial displacement adjustments of the internal simulated drill rod through threaded fittings and screws, ranging from -127.0 mm to 304.8 mm. The tool is designed to withstand both tensile and compressive forces during drilling.

**Simulated Conductor Casings:** Two types of simulated casings were employed to mimic the jetting installation process of conductor casings. The technical parameters of the deployed casing-column combinations, including the casing length, simulated casing outer diameter, simulated casing inner diameter, drill bit outer diameter, and adjustable extension range, are presented in [Table 2](#).

The simulated casings were designed as follows: For Exp. No. 1–3, the casing (Simulated Casing 1#) had an outer diameter of 127.0 mm and an inner diameter of 115.8 mm, with a scaling factor for the outer diameter of 7.2:1 and for the wall thickness of 4.5:1, relative to the commonly used 36-inch conductor casing in the South China Sea. This configuration was used to simulate the jetting installations in the upper low-strength soil layers. For Exp. No. 4–6, the casing (Simulated Casing 2#, 4 inches) had an outer diameter of 101.6 mm and an inner diameter of 88.6 mm, with a scaling factor for the outer diameter of 9:1 and for the wall thickness of 3.9:1, which was used to simulate jetting installations in lower high-strength soil layers. These scaling factors were selected carefully to ensure the reliability and applicability of the simulation results in real-world scenarios.

**Drill Rod and Stabilizing Subs:** The drill rod employed was of the standard type for engineering drilling machines, with an outer diameter of 42.0 mm and wall thickness of 4.0 mm. Drill rods of varying lengths were used to satisfy the design requirements for drill-bit extensions. Simulated stabilizing subs were utilized to maintain bit centrality during drilling, foster uniform soil disruption at the casing tip, effectively prevent wellbore deviation, and control well trajectories.

The assembly of the casing running system was designed to emulate the sequential configuration of a typical drilling operation. The assembly comprises a series of components arranged in the following order: drill bit, drill bit crossover sub, drill pipe pup joint, drill pipe stabilizer, crossover sub, drill collar, crossover sub, drill pipe, additional crossover sub, simulated CADA tool, simulated casing, crossover sub, drill pipe, and square drill pipe. This structured assembly design mirrors the string configuration observed in actual drilling operations, thereby ensuring the authenticity and reliability of the experimental simulation.

**Drilling Rig:** A soil-drilling rig with a drilling depth capacity of 150 m and powered by a main engine of 24 hp (approximately 18 kW) was utilized.

**Mud Pump:** The compact mud pump, BW-250, was selected for this

study. This pump, driven by an L28 diesel engine with a rated power of 20 kW and a rotation speed of 2200 rpm, has a maximum discharge capacity of 350 L/min, facilitating the delivery of the drilling fluid necessary for catheter installation.

**Measurement Sensors:** A sophisticated data acquisition system comprising precision instruments was deployed to collect real-time parameters during the jetting process. The system included the UNI-T390B laser displacement sensor (measurement range: 0–10 m, accuracy: 1.0 mm), the SIS426-90 high-precision dual-axis tilt sensor (resolution: 0.002°, accuracy: 0.02°), the XLY-TY02A micro earth pressure gauge (dimensions: 17 mm × 9 mm, range: 0–600 kPa, accuracy:  $\leq \pm 0.1\%$  F•S), and the DN50-N electromagnetic flow meter (range: 0–500 L/min, accuracy:  $\leq \pm 0.5\%$  F•S). Additionally, the system incorporates a drill pressure sensor, speed sensor, multichannel data collector, and data acquisition computer.

In the conductor casing assembly, XLY-TY02A micro earth pressure gauges were mounted on the outer wall at 0.5-m intervals. Eleven pressure gauges were arranged linearly along the casing from the base to the top. The calibration parameters of the soil pressure sensors, crucial for this study, are listed in [Table 3](#). These calibration values represent the characteristic responses of each device, ensuring the precision and consistency of each measurement. Accurate calibration is essential for the reliability of the pressure data—vital for the validity of subsequent multi-objective optimization analyses.

The experimental apparatus included a CADA tool, conductor casing, drilling rods, stabilizing subs, drilling rig, mud pump, and a comprehensive array of measurement sensors. These components were designed to simulate actual seabed conditions and the jetting installation process to ensure the accuracy and reliability of the data acquired during the experiments. This empirical support aids in understanding and optimizing the conductor casing jetting installation process.

### 3.1.3. Experimental process and drilling fluid displacement design

Drilling fluid is pivotal in the conductor casing jetting installation process. The precision in designing the flow rate significantly influences the experiment's success ([Kan et al., 2020](#)). Seawater, with a density of 1.03 kg/m<sup>3</sup>, was chosen as the drilling fluid due to its compatibility with the marine drilling environment, its cost-effectiveness, and its minimal environmental impact. This choice aligns with the industry standards for simulating offshore drilling conditions and ensures the ecological sustainability of the experimental setup. For example, the flow rate was less than 1.0% of the maximum designed flow rate when the actual drilling depth was set at 0.5% of the planned drilling depth. The flow rate was rapidly increased to the maximum designed value and was maintained throughout the jetting process. Upon reaching 95.0% of the planned drilling depth, the flow rate gradually decreased to 1.0% of the maximum design value and remained at this level until the completion of the conductor casing installation.

Throughout the experiment, modern sensor technologies were employed for real-time monitoring and recording of various parameters ([Geelen et al., 2021](#)). For example, pressure sensors were used to measure the internal jetting pressure of the conductor casing, displacement sensors were used to measure the downward movement of the conductor casing, and inclination sensors were used to ascertain the tilt of the conductor casing. Additionally, the jetting drilling time was determined by monitoring the installation speed at which the conductor casing

**Table 2**  
Technical parameters for deployed casing column combinations.

Exp. No.	Casing Length (m)	Simulated Casing OD (mm)	Simulated Casing ID (mm)	Drill Bit OD (mm)	Adjustable Extension Range (mm)
1	6.135	127	115.8	76	-127.0 mm–304.8 mm
2	6.516	127	115.8	60.3	-127.0 mm–304.8 mm
3	6.337	127	115.8	48.3	-127.0 mm–304.8 mm
4	11.602	101.6	88.6	76.0	-127.0 mm–304.8 mm
5	11.379	101.6	88.6	60.3	-127.0 mm–304.8 mm
6	11.534	101.6	88.6	48.3	-127.0 mm–304.8 mm

**Table 3**  
Calibration parameters for micro earth pressure gauges.

Instrument Number	#01	#02	#03	#04	#05
Calibration Coefficient	0.22956	0.23202	0.23234	0.22821	0.23373
Instrument Number	#06	#07	#08	#09	#10
Calibration Coefficient	0.21456	0.20782	0.23445	0.22001	0.23673
Instrument Number	#11				
Calibration Coefficient	0.22986				

descended. Installation speed is a pivotal metric for assessing the conductor casing installation efficiency. By varying parameters such as the drilling fluid flow rate, drill bit extension, and ratio of the drill bit to conductor casing size, the installation speeds under different soil strength conditions were recorded to analyze the factors affecting installation efficiency.

After the experiment, under certain recovery time conditions, the soil stress changes around the conductor casing and changes in the vertical ultimate bearing capacity of the conductor casing were monitored to determine the soaking time. The ultimate vertical bearing capacity of a conductor casing is a crucial parameter for assessing load-bearing stability. By setting the experimental conditions, the key influencing factors of the conductor casing load-bearing safety were analyzed, and the conductor casing soaking time data were documented.

Through meticulous control of the experimental process and drilling fluid flow rate design coupled with real-time monitoring using modern sensor technology, precise and practical data were gathered, offering robust support for the research and development of multi-objective deep reinforcement learning algorithms.

### 3.2. Data processing for conductor casing jetting installation

#### 3.2.1. Feature extraction of undrained shear strength of formation

To optimize the conductor casing jetting installation time using multi-objective deep reinforcement learning algorithms, the treatment and representation of the undrained shear strength features of the formation are crucial (Wang et al., 2022). As depicted in Fig. 2, directly inputting this feature into a neural network model poses several technical challenges owing to its dynamic nature across different layers and depths (Turkson and VandenBerge, 2023).

To address this issue, undrained shear-strength data from various layers and depths were processed as one-dimensional signals. An in-depth analysis was then conducted using the signal processing theory. This approach concentrates on the numerical characteristics of the data and highlights its sequential nature, effectively capturing its inherent features (Siddiqui et al., 2020; Yang et al., 2019; Bienen et al., 2010; Mbarak et al., 2020).

#### 3.2.2. Feature scaling for conductor casing jetting installation parameters

In optimizing the conductor casing jetting installation time using multi-objective deep reinforcement learning algorithms, addressing the feature scaling of installation parameters is crucial, particularly when

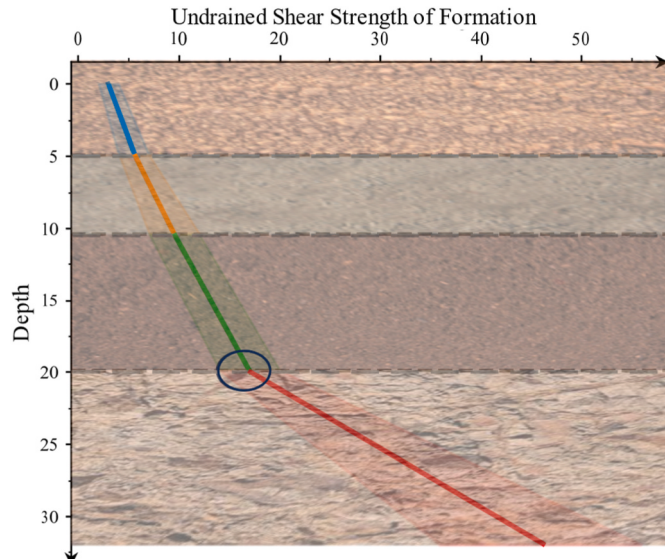


Fig. 2. Variation in the undrained shear strength of formation.

dealing with parameters of different magnitudes. Significant discrepancies in feature parameters, if fed directly into neural network training, may result in imbalanced gradient updates and distortion of the loss function shape, thereby affecting the optimization process's stability and efficiency (Bishop, 1995).

To resolve this problem, z-score standardization was employed to preprocess the feature parameters, ensure a uniform magnitude, effectively eliminate gradient update imbalances, and enhance the optimization stability of the loss function (Al Shalabi et al., 2006). Similarly, for the jetting, drilling, and soaking time data, the same treatment ensured that all data features possessed the same baseline magnitude during model training. This preprocessing strategy established a stable and consistent data environment for training the deep reinforcement learning model.

#### 3.2.3. Significance and correlation analysis of casing jetting installation parameters

In a study on optimizing the conductor casing jetting installation time using multi-objective deep reinforcement learning algorithms, significance and correlation analyses provided a foundational basis for feature selection (Bedi and Toshniwal, 2018).

Significance analysis employed the *t*-test, widely used to determine the statistical significance of differences between two sets of data averages. This analysis aims to identify feature parameters that have a significant impact on the conductor casing jetting installation time, thereby refining the feature selection within the model dataset. Following the significance analysis, a correlation analysis was performed using the Pearson correlation coefficient to evaluate the linear relationship strength between the feature parameters and the target variable (Kuhn and Johnson, 2013). This step establishes a foundation for model training and parameter optimization to ensure predictive accuracy and stability.

Fig. 3 illustrates how, through significance and correlation analysis, this study accurately identified feature parameters closely associated with the conductor casing jetting installation time, providing a more precise and consistent basis for predictions using the deep reinforcement learning model.

#### 3.2.4. Partitioning the casing jetting installation sample set

A comprehensive dataset comprising 1000 data points was systematically assembled through orthogonal experiments in surface conductor casing jetting installation simulations. Spanning a diverse range of

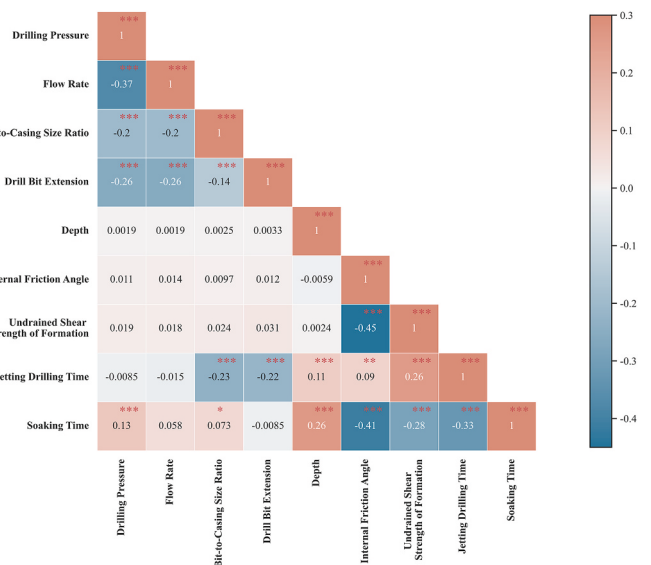


Fig. 3. Significance and correlation heatmap.

scenarios and parameter settings, this dataset provides a solid foundation for training and evaluating multi-objective deep reinforcement learning models.

To ensure the robustness and reliability of the model, a strategic partitioning approach was adopted by dividing the sample set into training, validation, and test sets at an 8:1:1 ratio. This ratio was selected to achieve a balance between a sufficiently large training set—crucial for capturing the complex relationships between the conductor casing jetting installation parameters and installation time, and adequate validation and test sets for model fine-tuning and performance assessment. Specifically, the validation set, constituting 10% of the data, played a pivotal role in model calibration and the detection of potential prediction biases. The test set, also comprising 10% of the data, was used exclusively to assess the model's performance on unseen data, ensuring its generalization capability (Joseph, 2022).

As shown in Fig. 4, an 8:1:1 partitioning ratio is standard practice in machine learning. This ratio ensures a balance between utilizing the data for learning and independently evaluating the model. By using a comprehensive dataset, this approach ensured that the training, validation, and test sets were representative and diverse. Consequently, the predictive accuracy and reliability of the developed model were enhanced in the context of conductor casing jet installation.

### 3.3. Analysis of factors influencing jetting drilling times

In the Conductor casing jetting installation experiments, multi-dimensional experimental data were systematically collected for jetting drilling and soaking times. These data encompass various formation characteristics and address a multitude of jet installation parameters. Based on these data, an in-depth discussion on the influence of various factors on the jetting drilling and soaking times was conducted.

#### 3.3.1. Influence of drilling pressure on jetting drilling time

By maintaining a constant flow rate, drill bit extension, and bit-to-casing size ratio, this study investigated the impact of varying the drilling pressure on the jetting drilling time and soaking time. As illustrated in Fig. 5(a), the jet drilling time decreased with increasing drilling pressure. Analysis of the interaction between the drill bit and formation revealed that an appropriate drilling pressure enhances the cutting effect of the drill bit on the formation, thereby improving the drilling efficiency. However, an increase in the drilling pressure might adversely affect the stability of the borehole wall, particularly in formations with unstable characteristics. Excessively high drilling pressures could lead to variations in pore pressures, potentially affecting the stability of the borehole and resulting in prolonged soaking time to ensure the stability of the surrounding rock.

#### 3.3.2. Influence of flow rate on jetting drilling time

With a constant drilling pressure, drill bit extension, and bit-to-casing size ratio, this study explored the impact of varying the flow rate on the jetting drilling and soaking times. As shown in Fig. 5(b), the jet drilling time progressively decreased with increasing flow rate. At

lower flow rates, the jetting drilling time was highly sensitive to changes in flow rate. However, after surpassing a certain threshold, this decreasing trend gradually tapered. An analysis of the interaction mechanism between the drill bit and formation revealed that the flow rate plays a crucial role in the rapid and efficient removal of cuttings as well as cooling and lubricating the drill bit. An optimal flow rate ensures maximum drilling efficiency while also mitigating the risks associated with blockages at the bottom of the hole due to cutting accumulation. Conversely, a low flow rate may hinder the orderly removal of cuttings, leading to an increase in the drill bit temperature and drilling resistance.

#### 3.3.3. Influence of drill bit extension on jetting drilling time

Under constant drilling pressure, flow rate, and bit-to-casing size ratio, the influence of varying the drill bit extension on the jetting drilling and soaking times was analyzed. As illustrated in Fig. 5(c), with an increase in the drill bit extension, the jetting drilling time first decreased, then sharply decreased, and eventually increased, indicating a minimum value for the jetting drilling time. According to the mechanism of interaction between the drill bit and formation, an appropriate extension can increase the contact area between the drill bit and formation, thereby enhancing the drilling efficiency. However, an extensive extension may reduce the stability of the drill bit when faced with complex marine geological structures, causing additional vibrations and impacts, which reduce the lifespan of the drill bit and affect the stability of the borehole wall.

#### 3.3.4. Influence of bit-to-casing size ratio on jetting drilling time

By maintaining a constant drilling pressure, flow rate, and drill bit extension, the effect of varying the bit-to-casing size ratio on the jetting drilling and soaking times was studied. As shown in Fig. 5(d), the jetting drilling time slowly decreased with an increase in the bit-to-casing size ratio but subsequently rebounded. Based on the interaction mechanism between the drill bit and formation, subtle changes in the bit-to-casing size ratio have significant effects on the drilling rates. An increase in the drill bit diameter with a corresponding increase in the borehole diameter may result in reduced lateral friction while descending the conductor casing, thereby enhancing the drilling speed. A higher size ratio can augment the contact area between the drill bit and formation, thereby improving the drilling efficiency. However, a larger size ratio may affect the efficiency of cutting removal as the effective flow space inside the conductor casing becomes limited, which may further affect the cooling and lubrication of the drill bit. The inappropriate selection of the bit-to-casing size ratio also increases the risk of borehole wall stability, particularly in marine environments with unique geological conditions and fracture distributions.

## 4. Multi-objective deep reinforcement learning algorithm for conductor casing jetting installation parameter optimization

To optimize the conductor casing jetting installation time effectively, this study first introduced a conductor casing jetting installation time prediction model based on a fully connected neural network algorithm. Based on this model, a Markov Decision Process (MDP) environment was established.

### 4.1. Times conductor casing jetting installation time prediction model

In deepwater drilling operations, the installation of a conductor casing involves two main phases: jetting drilling and soaking. The jetting drilling phase uses a water-jetting force to disperse the soil and create a borehole. The efficiency of this phase is influenced by various parameters such as the drilling pressure, flow rate, and drill bit extension. These parameters affect the soil disturbance around the casing, borehole quality, and the degree of borehole enlargement. They also affect the stress recovery process of the soil strength—crucial for the safety and efficiency of casing installation. In contrast, the soaking phase—

Sample set											
	Test set	Validation set	Training set								
	1st copy	2nd copy	3rd copy	4th copy	5th copy	6th copy	7th copy	8th copy	9th copy	10th copy	
1-Fold	1st copy	2nd copy	3rd copy	4th copy	5th copy	6th copy	7th copy	8th copy	9th copy	10th copy	
2-Fold	1st copy	2nd copy	3rd copy	4th copy	5th copy	6th copy	7th copy	8th copy	9th copy	10th copy	
3-Fold	1st copy	2nd copy	3rd copy	4th copy	5th copy	6th copy	7th copy	8th copy	9th copy	10th copy	
4-Fold	1st copy	2nd copy	3rd copy	4th copy	5th copy	6th copy	7th copy	8th copy	9th copy	10th copy	
5-Fold	1st copy	2nd copy	3rd copy	4th copy	5th copy	6th copy	7th copy	8th copy	9th copy	10th copy	
6-Fold	1st copy	2nd copy	3rd copy	4th copy	5th copy	6th copy	7th copy	8th copy	9th copy	10th copy	
7-Fold	1st copy	2nd copy	3rd copy	4th copy	5th copy	6th copy	7th copy	8th copy	9th copy	10th copy	
8-Fold	1st copy	2nd copy	3rd copy	4th copy	5th copy	6th copy	7th copy	8th copy	9th copy	10th copy	
9-Fold	1st copy	2nd copy	3rd copy	4th copy	5th copy	6th copy	7th copy	8th copy	9th copy	10th copy	

Fig. 4. Casing jetting installation sample set partitioning.

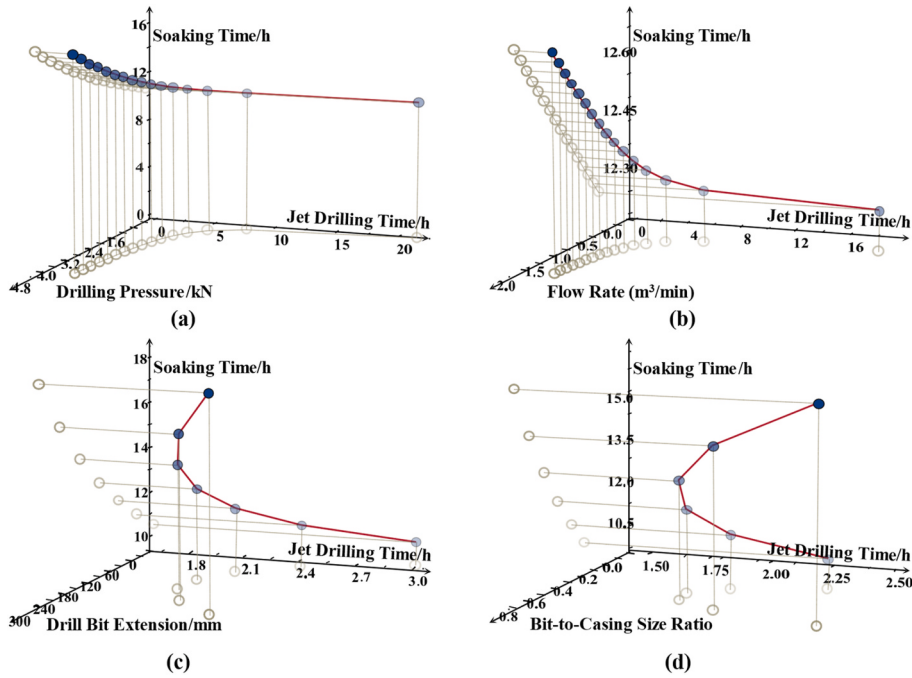


Fig. 5. Influence of various factors on jetting installation time.

referring to the time required for soil consolidation and strengthening after the casing installation—is vital for the stability and load-bearing capacity of the conductor casings. During this period, the surrounding soil compacted under the earth's stress, thereby providing adequate support for the conductor casing. In this study, the focus of the soaking time was specifically on the stress recovery period after the conductor casing was jetted to the designed depth and the running tool was released (soaking time from jetting completion to running tool release). This time is essential to ensure the stability of the conductor casing and its surrounding soil structure.

To simulate the actual conductor casing jetting installation process and accurately predict the installation time, a complex neural network model was designed and applied. The input features of this model are meticulously selected jetting installation parameters, including Drilling Pressure, Flow Rate, Drill Bit Extension, Undrained Shear Strength of Formation, and Internal Friction Angle. These features are believed to have a significant influence on the installation time of conductor casing jetting in real-world scenarios. The output of the model was designed to capture two critical time intervals during the jetting installation process: the jetting drilling and soaking times.

Owing to the characteristics of the input features and available training data, a fully connected neural network was chosen as the prediction model. This network is adept at capturing intricate mapping relationships between the input features and output. Dropout layers were added to mitigate overfitting and ensure model robustness, even with limited training data (Park and Kwak, 2017). The initial weights of the model were determined using Particle Swarm Optimization to avoid the local optima (Ye, 2017; Lorenzo et al., 2017). Hyperparameters such as the learning rate, number of neurons in the hidden layer, and dropout rate were optimized using a grid search approach (Tani et al., 2021).

With this strategic design, an effective prediction of the conductor casing jetting installation time was achieved, laying a solid foundation for subsequent multiobjective reinforcement learning algorithms.

#### 4.2. Markov Decision Process environment

The conductor casing jetting installation parameters were optimized by constructing a specific MDP environment. Given that the conductor

casing jetting installation process is a deterministic physical procedure, the state transition probabilities in this environment were set as constants.

##### 4.2.1. Reward function design

The reward function is a pivotal element in deep reinforcement learning that provides immediate feedback on the actions of multi-objective deep reinforcement learning algorithms, thus enabling the algorithm to gauge the consequences of its actions (Friedman and Fontaine, 2018). In the context of optimizing conductor casing jetting installations, the reward function must accurately reflect the impact of adjustments to the installation parameters on jetting outcomes.

**Jetting Drilling Time Reward:** This reward assesses the effectiveness of optimizing the conductor casing installation parameters based on the jetting drilling time derived from the prediction model. If an action resulted in a reduced drilling time, a positive reward was awarded. Conversely, if the drilling time increased, the reward was negative.

**Soaking Time Reward:** This reward evaluates stability during the conductor casing installation process based on the soaking time obtained from the prediction model. A shorter soaking time may indicate a more stable installation, thus meriting a positive reward. In contrast, a longer soaking time suggests instability, meriting a negative reward.

By combining these two rewards, an aggregate reward is generated that guides the multi-objective deep reinforcement learning algorithm in continuous parameter optimization throughout the learning process. The importance of these two rewards can be balanced based on their real-world significance. For instance, if the drilling-time efficiency is considered more critical than the stability indicated by the soaking time, the weight of the drilling-time reward can be set higher.

##### 4.2.2. State and action spaces

The state space effectively represents the current condition of the conductor casing jetting process, encompassing parameters such as the drilling pressure, flow rate, drill bit extension, and bit-to-casing size ratio. Conversely, the action space defines the boundaries within which jetting parameters can be adjusted (Zhu et al., 2021; Hausknecht and Stone, 2015). When an agent executes an action, it influences the existing environmental state and receives feedback from the dual reward

functions associated with the jet drilling and soaking times.

#### 4.2.3. Learning mechanism

This study introduces a multi-objective deep reinforcement learning algorithm based on composite action value Q-learning (CAPQL). This algorithm combines deep Q-learning with policy-gradient methods to provide an optimized approach for continuous action spaces.

**Online Q-Network and Target Q-Network:** The primary role of the online Q-Network is to evaluate the rewards corresponding to the prevailing conductor casing jet state. The inputs for the network included the current jetting parameters: Drilling Pressure, Flow Rate, Drill Bit Extension, and the Bit-to-Casing Size Ratio. In contrast, the outputs anticipate jetting, drilling, and soaking times for diverse actions under the existing state. The Online Q-Network is in a perpetual state of learning and updating, aiming to bridge the gap between its predicted installation time and the time projected from the conductor casing jet time prediction model. While mirroring the structure of the online Q-network, the Target Q-Network initializes its parameters using the weights of the latter. The essence of this network is offering a stable learning objective, thereby curtailing fluctuations during the learning phase. Throughout the learning process of the multi-objective deep reinforcement learning algorithm, the Target Q-Network parameters receive periodic updates by replicating the parameters of the Online Q-Network. This strategy enhances the stability of the learning process and increases the efficiency of the model.

**Policy Network:** The primary goal of this network is to pinpoint the most favorable action choice, given the conductor casing jet state. Upon receiving the specific jetting parameters, the policy network outputs a probability distribution across a gamut of actions. By leveraging this distribution, the model pinpoints the optimal action and computes a loss value by integrating predictions from both the Online and Target Q-Networks. This deduced loss aids in further refining the parameters of the Policy Network and the Online Q-Network. To ensure a seamless training trajectory, the parameters from the Online Q-Network were intermittently duplicated onto the Target Q-Network at designated junctures.

**Priority Experience Replay:** This mechanism plays an instrumental role in the learning curve of conductor casing jetting. Within this framework, the experience pool, which functions as a central repository for historical jetting states and correlated rewards, consistently supplies data for learning. A randomized sampling strategy guarantees balanced and unbiased learning across various jetting states, thereby fostering the model's adaptability and steadiness (Schaul et al., 2015). Of particular note is the priority-sampling methodology, which proficiently identifies experiences integral to the model's learning. Because each jetting state is related to varied jetting drilling times, some states may pose greater optimization challenges. By allocating an enhanced learning priority to these nuanced or unorthodox jetting states, the model is empowered to more adeptly fine-tune the parameters for these pivotal states, consequently boosting the overall optimization and consistency.

**Exploratory Noise Strategy:** This strategy assumes critical importance during the nascent phases of conductor casing jetting parameter optimization. In the elementary stages of the optimization voyage, this strategy propels the multi-objective deep reinforcement learning algorithm to extensively probe a plethora of potential jetting states (Plappert et al., 2017). As the depth of understanding of the optimization process is amplified, the strategy progressively veers toward jetting states that promise a reduced jetting drilling time, as predicted by the conductor casing jetting time prediction model.

#### 4.3. Pareto Frontier for jetting installation state

The concept of the Pareto frontier was introduced to address the inherently conflicting objectives of jetting drilling time and soaking time in conductor casing installations during deep-water drilling operations. These two phases were crucial for the efficiency and stability of the

installation process. Jetting-drilling time is affected by various factors, including jetting parameters and formation characteristics, whereas soaking time is vital for soil consolidation and strengthening after casing installation. Considering reducing both the jetting drilling and soaking times simultaneously is impossible, identifying an optimal balance between the two is essential.

The Pareto frontier defines a set of elite solutions in which improving one objective necessitates compromising another (Ngatchou et al., 2005; Ruchte and Grabocka, 2021). In the context of this research, these solutions represent the optimal balance between the jetting drilling time and soaking time. A Pareto-optimal solution should maintain a balance between these two time objectives, avoiding situations in which minimizing one time metric results in maximizing the other (Petchrompo et al., 2022).

During the training phase, non-dominated sorting methods were used to evaluate and filter the potential solutions (Yang et al., 2023). Each iteration of the multi-objective deep reinforcement learning algorithm produced a new batch of solutions based on the current state of jetting installation, which was influenced by factors such as drilling pressure, flow rate, bit-to-casing size ratio, and drill bit extension. These factors dictated the jetting drilling and soaking times. By comparing the quality of these solutions, solutions that qualified as Pareto optimal could be determined. A solution was considered Pareto-dominant if it was not inferior to another solution in all objectives, and superior in at least one objective. The set of Pareto-dominant solutions constituted the current Pareto frontier. The installation time model for the conductor casing jetting process was formulated as shown in Equation (1). To further analyze the factors influencing the installation time, we decomposed it into two distinct components: the jetting drilling time and soaking time. The jetting drilling time model is presented in Equation (2), and the soaking time model is described in Equation (3):

$$T_{\text{installation}} = T_{\text{jetting drilling}} + T_{\text{soaking}} \quad (1)$$

$$T_{\text{jetting drilling}} = f(P_{\text{drilling}}, Q_{\text{flow rate}}, L_{\text{bit extension}}, R_{\text{bit-to-casing ratio}}, \varphi, c) \quad (2)$$

$$T_{\text{soaking}} = f(P_{\text{drilling}}, Q_{\text{flow rate}}, L_{\text{bit extension}}, R_{\text{bit-to-casing ratio}}, \varphi, c) \quad (3)$$

The optimization framework developed in this study aims to balance the jetting, drilling, and soaking times by optimizing the installation parameters. The objective function and constraints of this framework are defined by Equation (4).

$$\begin{aligned} \min & \left\{ \begin{array}{l} T_{\text{installation}} \\ w_1 T_{\text{jetting drilling}} \\ w_2 T_{\text{soaking}} \end{array} \right. \\ \text{s.t. } & P_{\text{drilling}}, Q_{\text{flow rate}}, L_{\text{bit extension}}, R_{\text{bit-to-casing ratio}}, \varphi, c \end{aligned} \quad (4)$$

In the formula,  $T_{\text{installation}}$  is the total installation time (h);  $T_{\text{jetting drilling}}$  is the jetting drilling time (h);  $T_{\text{soaking}}$  is the soaking time (h);  $P_{\text{drilling}}$  is the drilling pressure (kN);  $Q_{\text{flow rate}}$  is the flow rate ( $\text{m}^3/\text{min}$ );  $L_{\text{bit extension}}$  is the drill bit extension (mm);  $R_{\text{bit-to-casing ratio}}$  is the bit-to-casing size ratio;  $\varphi$  is the internal friction angle ( $^\circ$ );  $c$  is the undrained shear strength (kPa);  $w_1$  and  $w_2$  are the optimization target weight coefficients.

The dynamic nature of the Pareto frontier is recognized as a crucial aspect of the optimization process (Chen et al., 2020). As each iteration may produce varied solutions, the boundary of the Pareto frontier is considered to be in constant flux. Continuous training of the multi-objective deep reinforcement learning algorithm along with regular refinement and optimization of the solution set gradually led to convergence toward the global Pareto frontier. Because of the conflicting objectives of jetting drilling time and soaking time, this dynamic optimization process places heightened demands on the training of the multi-objective deep reinforcement learning algorithm and evaluation of its solutions. This process highlights the complexity and challenges of achieving an optimal balance between jetting drilling time and soaking

time, underscoring the innovative and significant contribution of the multi-objective deep reinforcement learning algorithm to optimizing the conductor casing jetting installation parameters.

## 5. Training and validation

### 5.1. Training of conductor casing jetting installation time prediction model

The parameters for the jetting installation of the conductor casing refer to the maximum design values established before installation commenced. During the jetting drilling process, the jetting installation parameters were dynamically adjusted according to their respective strategies for the target wells within a given block, facilitating the completion of the conductor casing jetting installation.

#### 5.1.1. Training strategy

Considering the multi-output nature of the conductor casing jetting installation time prediction model, a weight coefficient loss function was introduced to adapt the loss function of the model. The loss function for this model is defined as shown in Equation (5).

$$\text{Loss} = \frac{1}{n} \left( \gamma_L \sum_{i=1}^n |y_J^{(i)} - \hat{y}_J^{(i)}| + (1 - \gamma_L) \sum_{i=1}^n |y_S^{(i)} - \hat{y}_S^{(i)}| \right) \quad (5)$$

where  $\text{Loss}$  represents the loss function of the model,  $n$  is the batch size,  $y_J$  denotes the true value of the jetting drilling time,  $\hat{y}_J$  is the predicted value of the jetting drilling time,  $y_S$  is the true value of the soaking time, and  $\hat{y}_S$  is the predicted value of the soaking time.

Particle Swarm Optimization (PSO) is employed to optimize the initial weights and biases of the model. Existing research indicates this method can significantly accelerate the convergence speed of the model compared to randomly initialized weights. To minimize the chance of the model being trapped in the local optima, a learning rate warm-up and cosine-annealing restart strategy was utilized during the training phase to adjust the training learning rate. Furthermore, to enhance the performance of the model, a grid search method was used during the validation phase to optimize specific training hyperparameters within a given range. To further alleviate the overfitting, early stopping was adopted during the validation phase to update the model. The range and optimization results of the training hyperparameters for the conductor casing jetting installation time prediction model are listed in Table 4.

The parameters set for the Particle Swarm Optimization algorithm are shown in Table 5.

The AdamW optimizer was used, and a flowchart of the training, validation, and testing processes for the conductor casing jetting installation time prediction model is depicted in Fig. 6.

#### 5.1.2. Training and validation process

The variation curves of the training and validation loss values with epochs during the training of the conductor casing jetting installation time prediction model are shown in Figs. 7 and 8, respectively.

Figs. 7 and 8 clearly demonstrate the trend of the loss value curve of the model with epochs. Between epochs 1–58, the loss-value curve converges rapidly. Entering epochs 58–77, the curve began to stabilize.

**Table 4**  
Training hyperparameter range and optimization results.

Hyperparameter Name	Range	Optimized Value
Initial Learning Rate	0.0010–0.0050	0.0025
Epochs	150~220	197
Loss Function Weight Coefficient	0.10–0.90	0.41
Batch Size	20~40	32
Dropout Rate	0.30–0.70	0.44
Weight Decay	0.0002–0.0005	0.0004

**Table 5**  
Parameters for particle swarm optimization algorithm.

Parameter Name	Parameter Description	Value
Swarm Size	Number of particles in the swarm.	40
Iterations	Total cycles before termination.	200
Inertia Weight	Influences particle's velocity persistence.	1
Personal Learning Factor	Weight on particle's best position.	1.5
Group Learning Factor	Weight on global best position.	2

However, during epochs 150–200, although the training loss value curve continued to decline, the validation loss value curve exhibited oscillations, suggesting a risk of model overfitting if the training persisted.

The Mean Square Error (MSE), Root Mean Square Error (RMSE), and Mean Absolute Error (MAE) were chosen as the evaluation metrics for the conductor casing jetting installation time prediction model. These metrics are defined in Equations (6)–(8), respectively.

$$MSE_{J/S} = \frac{1}{N} \sum_{i=1}^N \left( y_{J/S}^{(i)} - \hat{y}_{J/S}^{(i)} \right)^2 \quad (6)$$

$$RMSE_{J/S} = \sqrt{\frac{1}{N} \sum_{i=1}^N \left( y_{J/S}^{(i)} - \hat{y}_{J/S}^{(i)} \right)^2} \quad (7)$$

$$MAE_{J/S} = \frac{1}{N} \sum_{i=1}^N \left| y_{J/S}^{(i)} - \hat{y}_{J/S}^{(i)} \right| \quad (8)$$

The model evaluations using a test set of 50 samples are presented in Table 6.

A comparison of the values predicted by the model with the actual labels is shown in Figs. 9 and 10.

Figs. 9 and 10 clearly demonstrate the degree of proximity between the model's predicted values and the actual labels. The model's prediction for the jetting drilling time is more precise than that for the static time, suggesting a strong correlation between the jetting installation parameters and jetting drilling time.

Table 6, Figs. 9, and Fig. 10 confirm that the conductor casing jetting installation time prediction model trained on the deepwater surface conductor casing jetting installation experimental dataset can swiftly and accurately predict the jetting drilling and soaking time.

## 5.2. Multi-objective deep reinforcement learning algorithm training

For the target block at a water depth of 1400 m, a 914.4 mm surface casing was installed using the jetting method. Seabed soil quality data for this area were obtained by drilling and sampling, as listed in Table 7. In this phase of the study, geotechnical parameters such as the undrained shear strength were fixed to a specific set of values to focus on the optimization of the jetting installation parameters within the same stratum combination. The state and action spaces of the target well-casing jetting installation parameters are listed in Table 8.

### 5.2.1. Q-network and policy network training

The hyperparameters for training the Q-network and policy network using the multi-objective deep reinforcement learning algorithm are listed in Table 9.

The training phase primarily focuses on continuous updates of the Q-network and policy networks. For the Q-network, optimizers were used to minimize the mean squared error loss. This loss quantifies the discrepancy between the installation time predicted by the Q-network and the casing jetting installation time predicted by the model. Loss was recorded after each update, providing data support for the subsequent learning process analysis.

The update phase of the policy network is more intricate. First, the expected installation parameter changes were generated based on the current jetting installation state. These changes are then passed to each

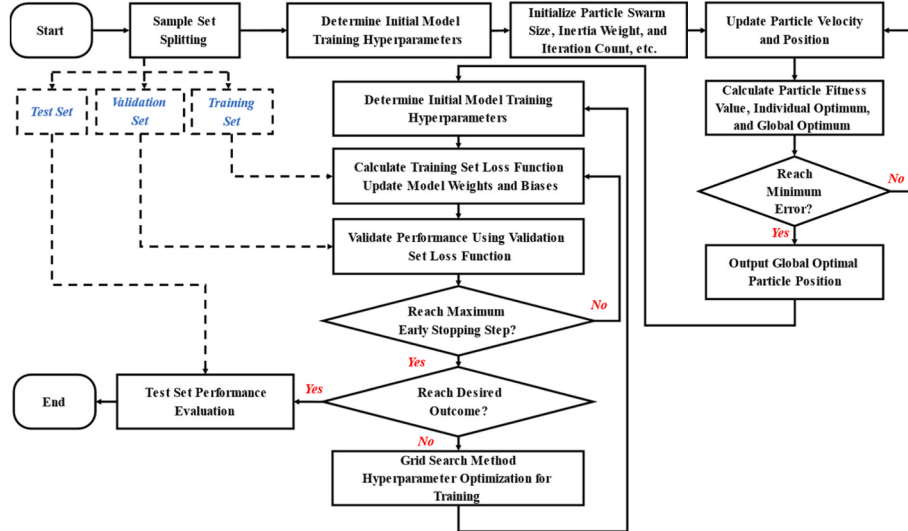


Fig. 6. Flowchart of training, validation, and testing for the prediction model.

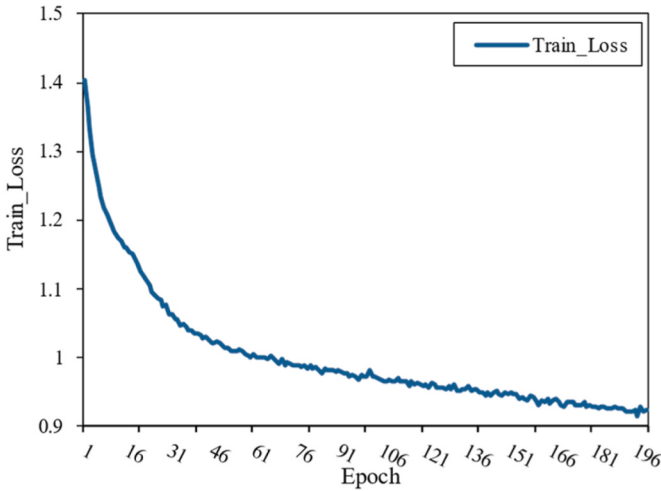


Fig. 7. Model training loss value curve.

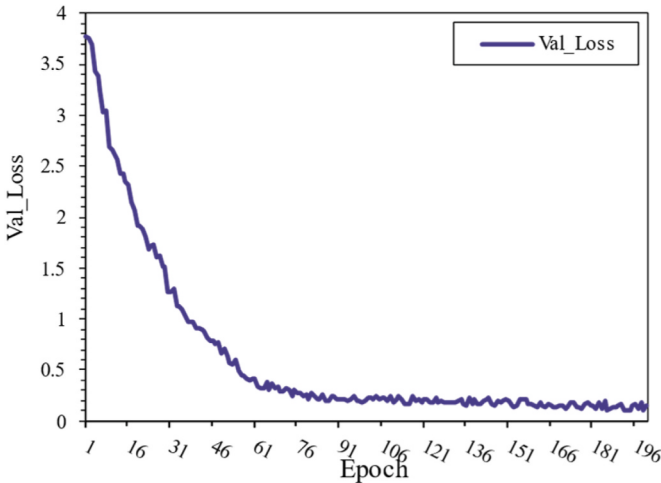


Fig. 8. Model validation loss value curve.

Table 6  
Evaluation results of the prediction model.

MSE J	MSE S	RMSEJ	RMSES	MAEJ	MAES	Test Time (s)
0.0294	0.0347	0.1714	0.1862	0.1725	0.1819	0.6811

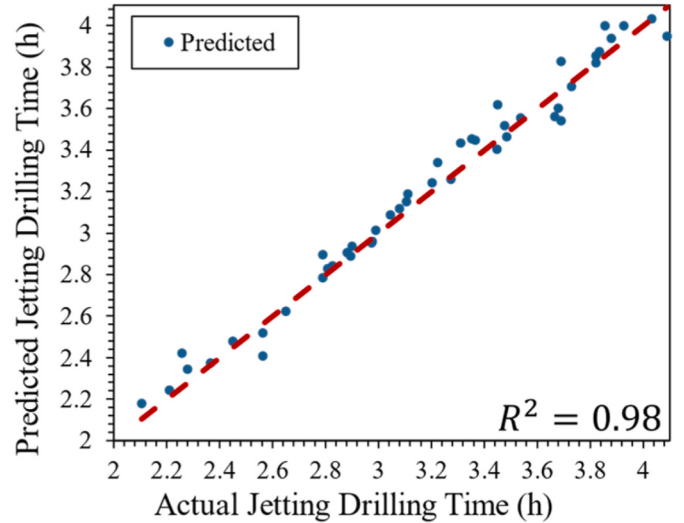
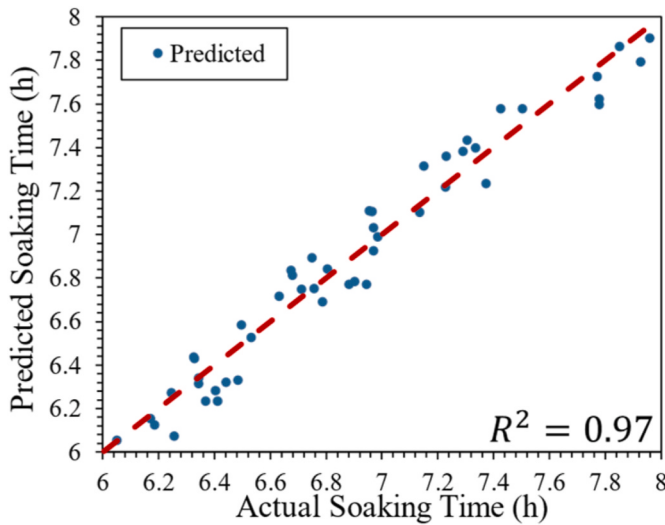


Fig. 9. Comparison between Model's drilling time predictions and actual labels.

Q-network, allowing the calculation of the expected mean squared error loss across all objectives. Thus, the loss in the policy network was derived. The optimizer subsequently backpropagates this loss, leading to adjustments in the network weights.

These network update strategies, whether for the Q-network or the policy network, aim to reduce the discrepancy between the predicted installation time and the casing jetting installation model and continually optimize the network weights. Together, these efforts enhanced the overall performance of the model. The ultimate research goal is to optimize the casing-jetting installation time more precisely. The loss curves of the Q-network and decision network training for the jetting, drilling, and soaking time objectives with respect to the epoch changes are shown in Figs. 11–13.



**Fig. 10.** Comparison between Model's static time predictions and actual labels.

**Table 7**  
Seabed soil parameters.

Top Depth (m)	Bottom Depth (m)	Soil Characteristics	Unit Weight ( $kN/m^3$ )	Top Undrained Shear Strength (kPa)	Bottom Undrained Shear Strength (kPa)
0.00	3.20	Clay	17.0	10	10
3.20	4.90	Clay	17.0	10	25
4.90	14.00	Clay	17.5	30	40
14.00	24.00	Clay	17.5	40	50
24.00	31.80	Clay	17.5	50	80
31.80	45.90	Clay	18.4	80	80
45.90	49.80	Clay/Sand	19.0	110	110
49.80	51.20	Clay	18.6	115	115
51.20	58.00	Clay	18.8	100	100
58.00	67.60	Clay	18.5	130	130
67.60	72.80	Clay	19.0	130	140
72.80	82.40	Clay	19.0	150	200
82.40	108.00	Clay	19.5	270	360

**Table 8**  
State space and action space range.

Parameter Category	Parameter Name	Space Range
State Space	Drilling Pressure (kN)	[1.0, 5.0]
	Flow Rate ( $m^3/min$ )	[0.6, 5.0]
	Drill Bit to Casing Size Ratio	[0.6, 0.8]
	Drill Bit Protrusion (mm)	[0.0, 300]
Action Space	Change Value	[-1.0, 1.0]

Figs. 11–13 depict the training loss descent curves for the Target 1 Q-Network, Target 2 Q-Network, and Policy Network, respectively, within the multi-objective deep reinforcement learning framework. Throughout the training process, all three networks exhibited fluctuating yet overall declining trends in training loss, indicating the convergence of the learning algorithm toward optimal policy identification.

Fig. 11 illustrates the training loss trajectory for Target 1 Q-network. Despite periodic fluctuations, there was a clear downward trend, demonstrating the network's increasing proficiency in approximating the state-action value function for one set of objectives in the conductor casing jetting installation domain. The oscillations present within the curve suggest an exploration-exploitation trade-off as the network refines its predictions through successive iterations.

**Table 9**  
Hyperparameters setting for Q-Network and policy network.

Hyperparameter	Hyperparameter Description	Value
policy_learning_rate	Learning rate of the policy network (policy_net) for updating the parameters of the policy network.	0.000005
q1_learning_rate	Learning rate of Q1 network for updating parameters of each Q network.	0.000005
q2_learning_rate	Learning rate of Q2 network for updating parameters of each Q network.	0.000001
gamma	Discount factor in reinforcement learning algorithms, used to measure the weight between current reward and future reward.	0.7
tau	Parameter for soft updating target network parameters, used for smoothly updating the target network.	0.7
weights	Weights for each optimization objective, used to weigh the importance of different objectives in the loss function.	0.8, 0.2
batch_size	Number of samples per batch in the experience replay buffer.	2048
buffer_size	Maximum capacity of the experience replay buffer for storing previous experience samples.	16,000
max_steps	Maximum number of steps executed in each epoch.	1000
alpha	Exponential parameter in the priority computation of the experience replay buffer.	0.6
beta_start	Initial importance sampling parameter in the priority computation of the experience replay buffer.	0.4
beta_end	Final importance sampling parameter in the priority computation of the experience replay buffer.	1
beta_decay	Decay steps for the importance sampling parameter in the priority computation of the experience replay buffer.	500

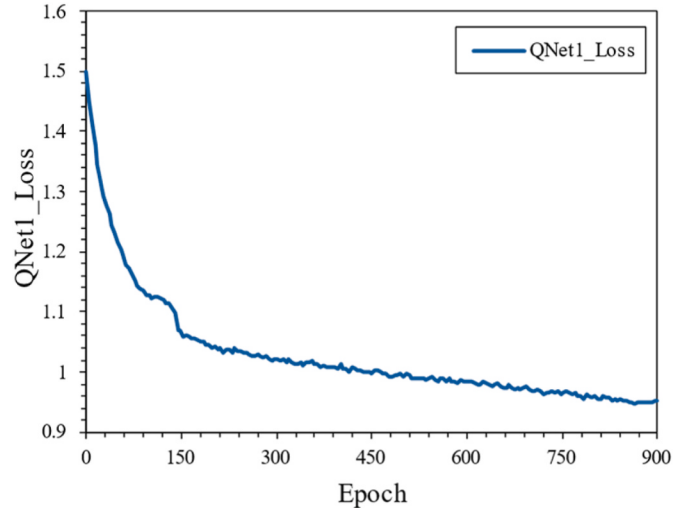


**Fig. 11.** Target 1 Q-Network training loss curve.

Similarly, Fig. 12 shows the training loss for the Target 2 Q-network. The profile of this curve echoes the learning behavior observed in the Target 1 Q-Network, with comparable variability and a definitive decremental pattern.

Fig. 13 shows the loss curve for the Policy Network—tasked with selecting actions that balance the competing objectives represented in the Target Q-Networks. The declining loss curve illustrates the Policy Network's maturation in identifying actions that progressively minimize the expected loss for both objectives concurrently. The exhibited fluctuations are characteristic of a complex decision-making environment, where the Policy Network navigates through a multi-dimensional

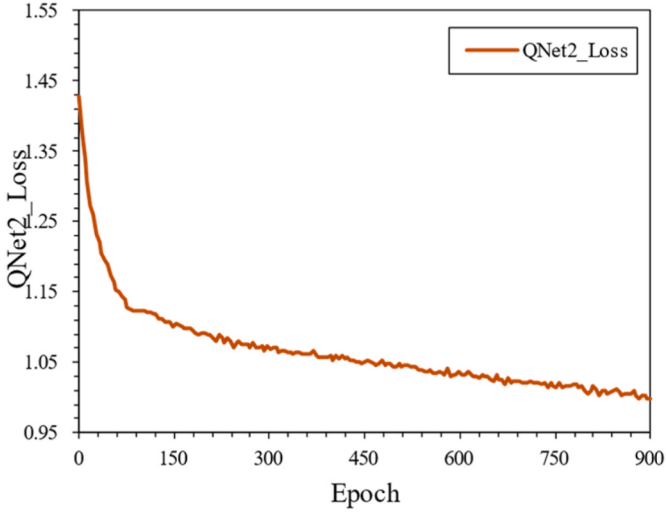


**Fig. 12.** Target 2 Q-Network training loss curve.

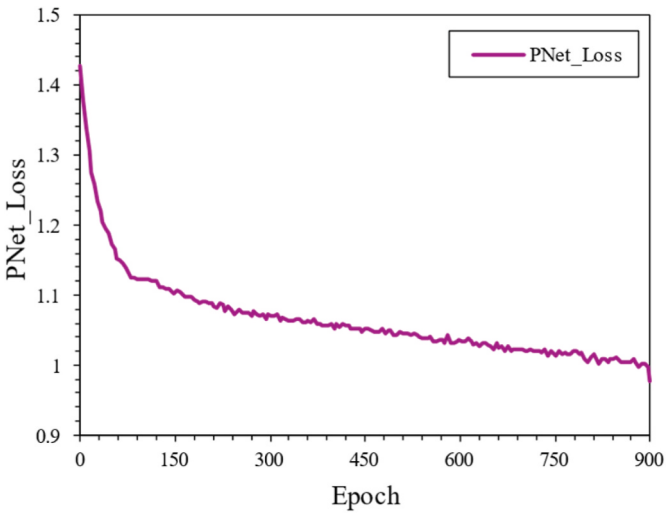


**Fig. 13.** Policy network training loss curve.

objective space to find a policy that synergizes the tradeoffs between different operational goals.

#### 5.2.2. Optimization process of conductor casing injection installation parameters

The variation in the jet drilling time across iterations is illustrated in Figs. 14 and 15.

Figs. 14 and 15 show the trends in changes in the jetting drilling time and soaking time during the iterations. In the initial iteration stages (not exceeding 50 iterations), the scatter plots of both variables displayed distinct diffusion characteristics. This observation hints at extensive sample collection within the state space using the exploratory noise strategy of the multi-objective deep reinforcement learning algorithm. As we transitioned to the mid-iterations (from 50 to 100 iterations), the scatter plot of the jetting drilling time initially showed an upward trend, followed by a descent, whereas the soaking time exhibited the opposite pattern: a decline followed by an ascent. These alterations suggest that although the overall jetting time has a decreasing trend, the optimization directions of the jetting drilling time and soaking time are not consistent during this phase. In the later stages of the iteration (from 100 to 400 iterations), the scatter plots of both the jetting drilling time and soaking time revealed a significant drop. This trend indicates that the

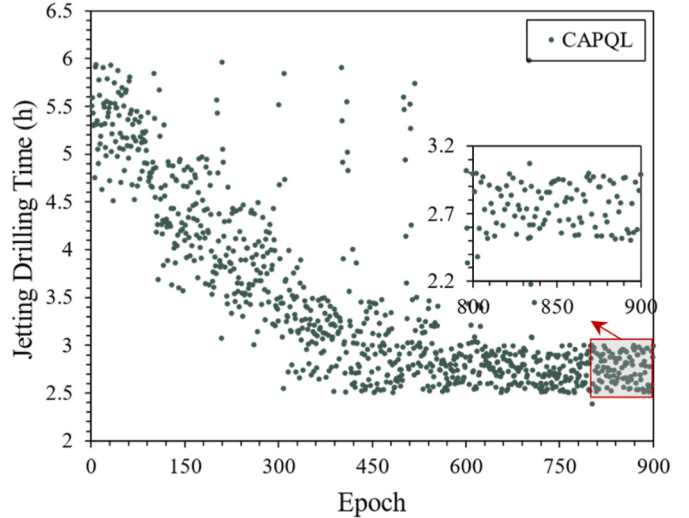


**Fig. 14.** Variation of jetting drilling time with iteration.

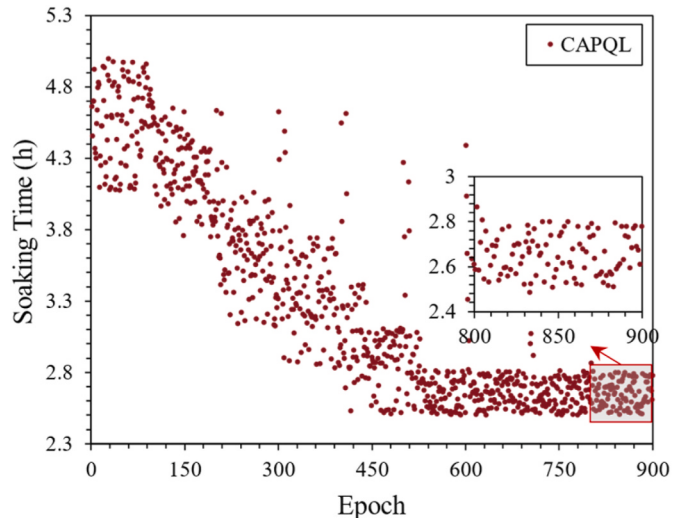


**Fig. 15.** Variation of soaking time with iteration.

degree of fit between the online Q-network and the conductor casing jetting installation time prediction model gradually intensified, leading to a more consistent optimization direction. By the end of the iteration period (from 400 to 900 iterations), the scatter plots for both time variables stabilized, suggesting that both the jetting drilling time and soaking time converged to their optimal values.

Scatter plots displaying the changes in various optimization parameters throughout the iteration process are shown in Figs. 16–19.

Figs. 16–19 provide detailed representations of the scatter plot distributions of the parameters across the iterations. During the initial iteration phase, specifically within the first 50 iterations, the scatter plot distributions for the Drilling Pressure, Flow Rate, Bit-to-Casing Size Ratio, and Drill Bit Extension values all displayed roughly uniform characteristics, thus validating the extensive sampling of the state space using the exploratory noise strategy of the multi-objective deep reinforcement learning algorithm. Moving into the mid-iterations, specifically up to the 400th iteration, the distribution of each parameter begins to display distinct characteristics: the scatter distribution of the Drilling Pressure is predominantly concentrated in the upper regions, the Flow Rate leans toward the upper-middle distribution, the Bit-to-Casing Size Ratio primarily resides in the lower-middle section, and the Drill Bit Extension distribution mainly focuses in the middle,

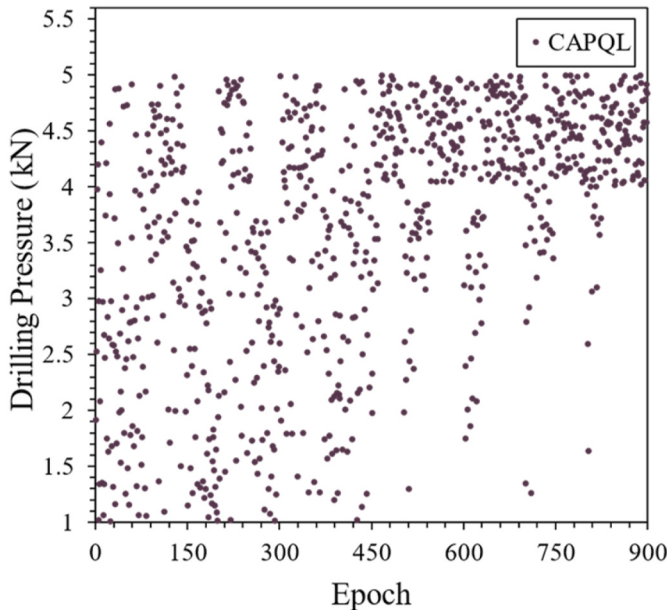


**Fig. 16.** Variation of Drilling Pressure with iteration.

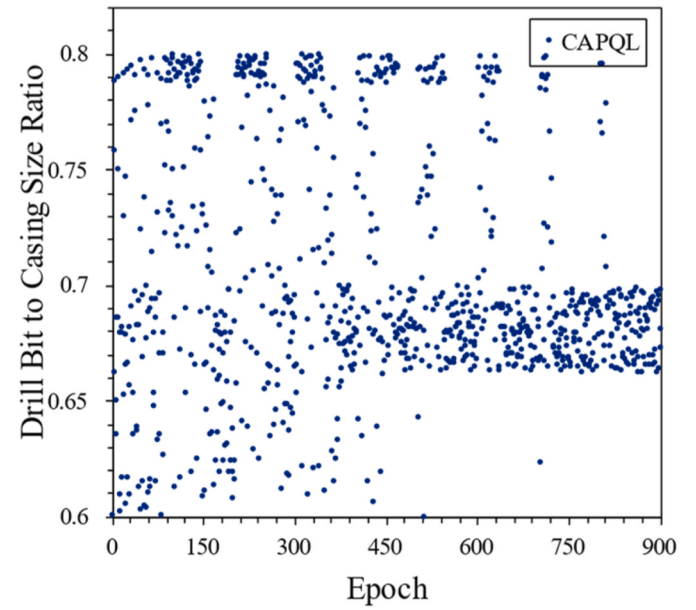


**Fig. 18.** Variation of Bit-to-Casing Size Ratio with iteration.

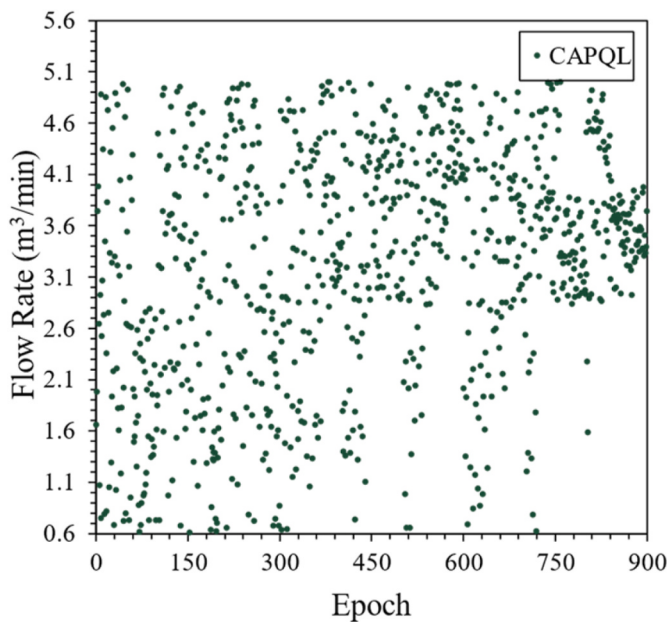


**Fig. 17.** Variation of Flow Rate with iteration.

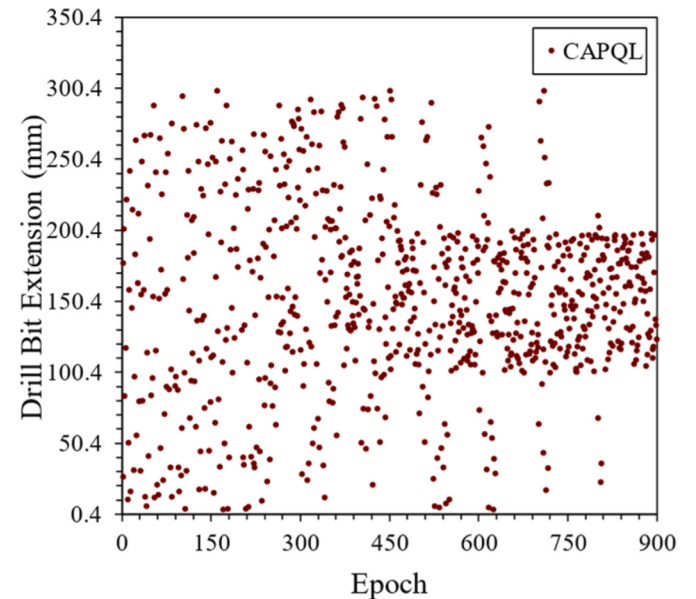


**Fig. 19.** Variation of Drill Bit Extension with iteration.

suggesting that the potential optimal intervals for each jet installation parameter were determined. During the subsequent iteration phases, from the 400th to the 900th iterations, the algorithm further refined the optimal intervals for each parameter, aiming to achieve optimal effects in the conductor casing jetting installation.

## 6. Case study analysis

Optimization was carried out specifically for the target wells in the designated block based on the design process for optimizing the conductor casing jetting installation parameters. The initial conductor casing jetting installation parameters for the target well before optimization are listed in Table 10.

The Pareto frontier after the optimization and variations in the installation parameters before and after optimization are depicted in

**Table 10**  
Initial conductor casing jetting installation parameters for target well.

Parameter Category	Parameter Name	Parameter Setting
Installation Parameters	Drilling Pressure (kN)	2.53
	Flow Rate (m³/min)	2.04
	Bit-to-Casing Size Ratio	0.65
	Drill Bit Extension (mm)	288.54
Installation Time	Initial Jetting Drilling Time (h)	5.39
	Initial Soaking time (h)	6.21

Figs. 20 and 21, respectively.

Fig. 20 shows the Pareto frontier for conductor casing jetting installation parameter optimization in the target block. This frontier delineates the optimal tradeoffs among the different jetting installation parameters. Fig. 21 shows the optimal points selected on the Pareto

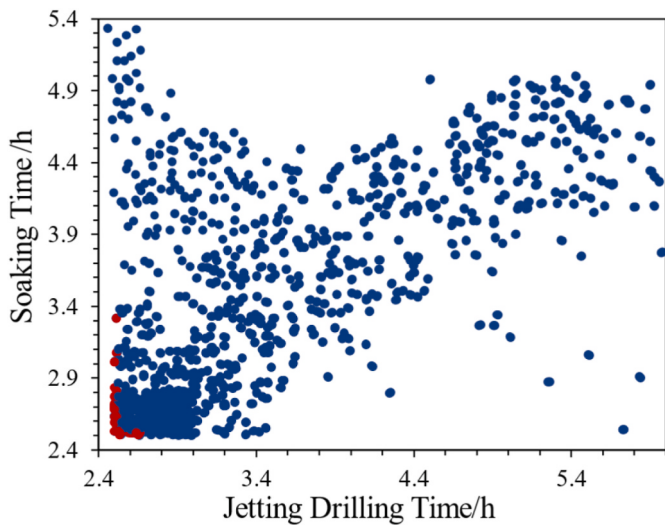


Fig. 20. Pareto frontier upon optimization completion.

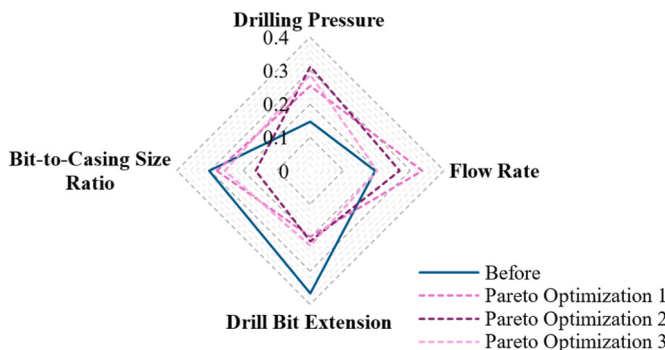


Fig. 21. Comparison of jetting installation parameters before and after optimization.

frontier with the pre-optimized conductor casing jetting installation parameters. Notably, the post-optimization values for the drilling pressure and flow rate exhibited significant increases, indicating a potential enhancement in jetting efficiency. Conversely, the bit-to-casing size ratio and drill bit extension values discernibly decreased, which could be associated with more precise control over the jetting drilling process.

To demonstrate the impact of the optimization, Table 11 presents a comparison of the conductor casing jetting installation parameters

**Table 11**  
Conductor Casing Jetting Installation Parameters: Pre-Optimization vs. Post-Optimization.

Parameter Category	Parameter Name	Pre-Optimization	Pareto Result 1	Pareto Result 2	Pareto Result 3
Installation Parameters	Drilling Pressure (kN)	2.53	4.36	5.36	4.96
	Flow Rate (m <sup>3</sup> /min)	2.04	3.51	2.81	2.11
	Bit-to-Casing Size Ratio	0.65	0.59	0.34	0.54
	Drill Bit Extension (mm)	288.54	155.34	166.34	176.34
Installation Time	Initial Jetting Drilling Time (h)	5.39	2.75	2.14	2.41
	Initial Soaking Time (h)	6.21	5.03	5.99	5.18

before and after the optimization process. The table includes the initial settings and three sets of results from the Pareto optimization, showing the parameter adjustments under various optimization objectives.

Notably, different combinations of jetting installation parameters can lead to varied outcomes concerning jetting drilling and soaking times. For instance, a higher drilling pressure and flow rate can reduce the jetting drilling time owing to the increased force and efficiency of fluid displacement. However, these factors might also have implications for the soaking time, potentially requiring a longer period for the displaced materials to settle owing to the induced turbulence. However, modifications in the bit-to-casing size ratio and drill bit extension can directly affect the drilling accuracy and subsequent soaking time. A smaller bit-to-casing size ratio and reduced drill bit extension might promote faster soaking because there is less disruption to the formation. These interdependencies underscore the significance of Pareto optimization in determining a balanced set of parameters that can offer optimal jetting installation performance while minimizing potential tradeoffs.

Comparisons of the jetting drilling time and soaking time before and after optimization are illustrated in Figs. 22 and 23, respectively.

Consolidating the insights from Figs. 22 and 23, for the target well, this procedure accomplished the optimization tasks for the jetting, drilling, and soaking times.

## 7. Conclusion

A vast array of data pertaining to the conductor casing jetting installation process was obtained through deep-water surface conductor casing jetting installation simulation experiments and subsequently compiled into a sample set. A prediction model for the conductor casing jetting installation time trained on this sample set was proposed. This model can accurately and efficiently emulate the mapping rules among the conductor casing jetting installation parameters, jetting drilling time, and soaking time.

Starting from the conductor casing jetting installation time prediction model and considering the actual engineering constraints of the conductor casing jetting installation parameters, the influence mechanism of the installation parameters on the installation time was explored, laying a theoretical foundation for the optimization of the conductor casing jetting installation parameters.

To minimize the conductor casing jetting installation time, a multi-objective deep reinforcement learning algorithm was employed to optimize the design of the conductor casing jetting installation parameters, culminating in a structured set of conductor-casing jetting installation parameter optimization design processes. Through

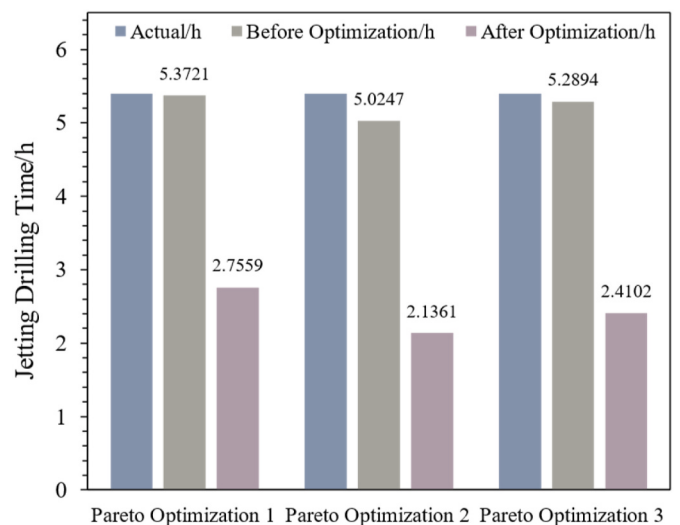


Fig. 22. Comparison of jetting drilling time before and after optimization.

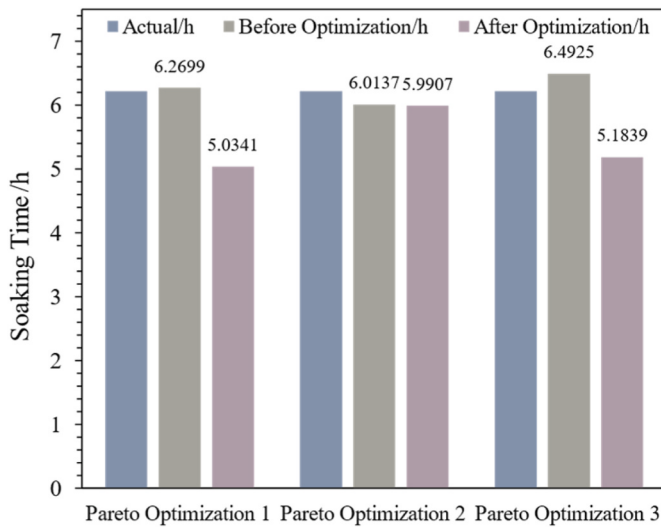


Fig. 23. Comparison of soaking time before and after optimization.

systematic experimentation under a target well in a specific block, a Pareto frontier was established to optimize the conductor casing jetting installation parameters. Several sets of jetting installation parameter combinations on this Pareto frontier demonstrate the potential to reduce the conductor casing jetting installation time optimally. More importantly, this process is universally applicable to different soil bodies for optimizing the conductor casing installation time.

However, these promising experimental results were based on certain assumptions and laboratory conditions. The real-world applicability of the optimized parameters inevitably leads to complexities and variabilities inherent to onsite conditions. Therefore, subsequent steps would entail rigorous field testing to validate and refine the findings of this study. Such on-site validations are crucial to ensure that the optimization processes developed in controlled environments translate

effectively into practical scenarios, accounting for unforeseen challenges and real-time adjustments. Nevertheless, the holistic and pragmatic utility of the optimized conductor casing jetting installation parameters was ensured through a continuous cycle of laboratory experimentation and field validation.

#### CRediT authorship contribution statement

**Yu Song:** Writing – review & editing, Validation, Supervision, Project administration, Methodology, Investigation, Funding acquisition. **Zehua Song:** Writing – review & editing, Writing – original draft, Visualization, Validation, Software, Methodology, Investigation, Formal analysis, Data curation. **Jin Yang:** Writing – review & editing, Project administration, Funding acquisition, Data curation, Conceptualization. **Lei Li:** Writing – original draft, Methodology, Investigation, Formal analysis.

#### Declaration of competing interest

The authors declare that they have no known competing financial interests or personal relationships that could have appeared to influence the work reported in this paper.

#### Data availability

The data that has been used is confidential.

#### Acknowledgements

This work was supported by the Hainan Province Major Science and Technology Plan Project “Research on Key Drilling Technologies for Natural Gas Hydrates” (No. ZDKJ2020011), the National Natural Science Foundation of China (No. 52204017), and the National Key Research and Development Program (No. 2022YFC28061004).

## Appendix A. Supplementary data

Supplementary data to this article can be found online at <https://doi.org/10.1016/j.oceaneng.2024.118398>.

## Appendix 1 Bearing Capacity Model for Conductor Casing

The calculation of the real-time bearing capacity of conductor casings often relies on empirical formulas, where the determination of empirical coefficients and bearing capacity recovery factors can vary significantly depending on soil conditions and construction conditions. A commonly used real-time bearing capacity formula in China, is described in Equation (A1).

$$Q_m = Q_i + \alpha(1 + \log T)(Q_{um} - Q_i) \quad (\text{A1})$$

In the equation,  $Q_m$  represents the real-time bearing capacity of the conductor casing at time  $m$  (kN);  $Q_i$  denotes the initial bearing capacity of the conductor casing (kN);  $\alpha$  is the lateral bearing capacity recovery coefficient, which is influenced by the conductor casing jetting process and installation conditions;  $T$  stands for the stress recovery time (min); and  $Q_{um}$  refers to the ultimate lateral bearing capacity of the conductor casing, which is the sum of the end bearing capacity and lateral resistance (kN).

The installation of the conductor casing can be considered as the bearing characteristics of a large-diameter non-displacement pile. During the installation process, due to the large diameter of the borehole, some of the confining pressure around the borehole dissipates, leading to a reduction in the frictional resistance of the soil against the casing walls. Furthermore, the larger the diameter of the casing, the more pronounced the dissipation of confining pressure, resulting in a greater reduction in lateral resistance.

The vertical ultimate bearing capacity of the conductor casing exhibits time-dependent behavior, increasing with time and eventually approaching a certain limit value. This time-dependent nature of the bearing capacity is mainly influenced by the thixotropic effect of the soil, the consolidation time effect, and the degree of soil disturbance. The installation of the conductor casing is affected by jetting disturbance factors, leading to the softening of lateral resistance around the casing, which results in a significant reduction in lateral resistance. After installation, as the surrounding soil recovers its stress, consolidates, and regains strength, the lateral resistance model of the casing wall can be described in Equation (A2).

$$Q_m = k \cdot Q_{um} \quad (\text{A2})$$

In the equation,  $k$  represents the softening coefficient of the bearing capacity of the casing wall, dimensionless.

The degree of disturbance of the soil around the casing is related to the jetting parameters. According to the momentum theorem, the force exerted on the soil is proportional to the square of the drilling fluid flow rate. The impact factor of the flow rate on the lateral resistance of the casing can be described in Equation (A3).

$$k_{jet} = \left( \frac{Q_{min}}{Q_a} \right)^2 \cdot \ln T \quad (A3)$$

In the equation,  $Q_{min}$  represents the minimum flow rate required for jetting and carrying cuttings ( $m^3/min$ ),  $Q_a$  denotes the average flow rate during the casing installation process ( $m^3/min$ ), and  $T$  stands for the soaking time of the casing (min).

Considering the influence of the drill bit extension on the bearing capacity of the casing, the impact factor can be described in Equation (A4).

$$k_{st} = \frac{d_{in}^2}{4[R_0 + (S - L)\tan(\frac{\alpha}{2})]^2} \cdot \ln T \quad (A4)$$

In the equation,  $d_{in}$  represents the internal diameter of the casing (m),  $L$  denotes the extension of the drill bit in the casing assembly (m), and  $\alpha$  stands for the jetting angle of the drill bit (degrees).

Integrating the factors of stress recovery time, flow rate, and casing assembly structure, the softening coefficient of the lateral bearing capacity of the casing during the jetting installation process can be described in Equation (A5).

$$k = A \left( \frac{Q_{min}}{Q_a} \right)^2 \cdot \ln T + B \frac{d_{in}^2}{4[R_0 + (S - L)\tan(\frac{\alpha}{2})]^2} \cdot \ln T \quad (A5)$$

In the equation,  $A$  and  $B$  are empirical coefficients, which are dimensionless.

Substituting the undetermined coefficients into the above formula, the real-time bearing capacity model of the conductor casing can be described in Equation (A6).

$$Q_m = \left\{ A \left( \frac{Q_{min}}{Q_a} \right)^2 \cdot \ln T + B \frac{d_{in}^2}{4[R_0 + (S - L)\tan(\frac{\alpha}{2})]^2} \cdot \ln T \right\} \cdot \left( \int_0^L \pi d_0 f dx + q_u A_0 \right) \quad (A6)$$

From the real-time bearing capacity model expression, it is evident that as the depth increases, the frictional force per unit area between the conductor casing and the soil increases, while the cross-sectional area of the conductor casing is relatively small, resulting in limited increase in end bearing capacity. Therefore, the bearing capacity of the conductor casing is mainly influenced by lateral frictional force, which is also crucial for the installation time of the conductor casing. Since the lateral frictional force of the conductor casing varies with the properties of the soil, it is necessary to calculate the frictional force for different soil types.

**Calculation of Unit Area Frictional Force in Clay Layers for Conductor Casing** The unit area frictional force of the conductor casing in clay layers can be considered as a function of the undrained shear strength of the soil, can be described in Equation (A7).

$$f_u = \alpha s_u \quad (A7)$$

In the equation,  $\alpha$  represents the adhesion coefficient, with a value less than or equal to 1, and  $s_u$  denotes the undrained shear strength of the soil, measured in pascals (Pa).

According to the API-RP-2A standard (2000 edition), the determination method can be described in Equation (A8).

$$\begin{cases} \alpha = 0.5\psi^{0.5}, & \text{if } \psi \leq 1.0 \\ \alpha = 0.5\psi^{-0.25}, & \text{if } \psi > 1.0 \\ \psi = \frac{s_u}{\sigma_v} \end{cases} \quad (A8)$$

In the equation,  $\sigma_v$  denotes the effective overburden stress in pascals (Pa). For the calculation of the unit area frictional force in clay layers, the strength value of remolded soil is typically employed. If the strength values of remolded soil are not available, half of the strength value of undisturbed soil is utilized instead.

**End Bearing Capacity of Conductor Casing in Clay Layers** The formula for calculating the end bearing capacity per unit area of the conductor casing in clay layers can be described in Equation (A9).

$$q_u = N_c s_u \quad (A9)$$

In the equation,  $N_c$  represents the bearing capacity coefficient for the conductor casing's unit area end resistance in clay layers. It is typically assumed to be 9 to account for the soil's ability to support the casing's load. This coefficient plays a crucial role in determining the overall bearing capacity of the conductor casing in soft soil conditions.

**Unit Area Frictional Force in Sandy Soil Layers** When the conductor casing is installed in sandy soil layers, the frictional resistance between the soil and the casing surface can be described in Equation (A10).

$$f_u = K\sigma_y \tan \delta \quad (\text{A10})$$

In the equation,  $K$  denotes the lateral earth pressure coefficient, which varies between 0.5 and 1 for axial compression loads, reflecting the soil's resistance to lateral movement. The friction angle  $\delta$  between the soil and the conductor casing is typically calculated as  $\delta = \varphi - 5$ , where  $\varphi$  is the soil's internal friction angle.

**End Bearing Capacity of Conductor Casing in Sandy Soil Layers** The formula for calculating the end bearing capacity per unit area of the conductor casing in sandy soil layers can be described in Equation (A11).

$$q_u = N_p P_0 \quad (\text{A11})$$

In the equation,  $N_p$  represents the bearing capacity coefficient. It is evident from the equation that the value of  $q_u$  is directly proportional to  $P_0$ , which increases linearly with the depth of the soil layer. However, beyond a certain critical depth, the increase in  $q_u$  with depth is no longer linear.

## Appendix 2 Detailed Test Parameters and Soil Characteristics for Conductor Casing Jetting Installation Experiments

**Table A1**

Comprehensive Overview of Test Parameters and Soil Characteristics for Test Scenario in the Target Block.

No.	Soil Description	Top Depth (m)	Bottom Depth (m)	Effective Unit Weight (kN/m³)	Design Shear Strength Lower Limit (kPa)	Design Shear Strength Upper Limit (kPa)	Design Shear Strength Average (kPa)	Drilling Pressure Lower Limit (kN)	Drilling Pressure Upper Limit (kN)	Flow Rate Lower Limit (m³/min)	Flow Rate Upper Limit (m³/min)	Drill Bit Extension (mm)	Bit-to-Casing Size Ratio
1	Very Soft High Plasticity Silty Clay	0	5	3	4	8.5	7	-	-	-	-	167	0.35
1	Very Soft High Plasticity Silty Clay	5	7.9	3	8.5	11	10	5.5	6.2	2.5	3.2	167	0.35
2	Soft to Moderately Hard High Plasticity Silty Clay	7.9	12.9	5.5	11	13	12	6.3	6.7	3.2	3.5	167	0.35
2	Soft to Moderately Hard High Plasticity Silty Clay	12.9	17.9	5.5	13	23	18	6.8	7	3.5	3.7	167	0.35
2	Soft to Moderately Hard High Plasticity Silty Clay	17.9	22.9	5.5	23	33	28	7.1	7.3	3.7	3.9	167	0.35
2	Soft to Moderately Hard High Plasticity Silty Clay	22.9	27.9	5.5	33	43	38	7.4	7.8	3.9	4.2	167	0.35
2	Soft to Moderately Hard High Plasticity Silty Clay	27.9	32.9	5.5	43	47.5	45	8.1	8.5	4.2	4.5	167	0.35
2	Soft to Moderately Hard High Plasticity Silty Clay	32.9	37.9	5.5	47.5	50.5	49	8.1	8.5	4.2	4.5	167	0.35
2	Soft to Moderately Hard High Plasticity Silty Clay	37.9	38	5.5	50.5	50.5	50.5	8.1	8.5	4.2	4.5	167	0.35
3	Moderately Hard to Hard Silt Clay	38	43	6	41	45.5	43.25	6.5	6.9	3	3.4	167	0.35
3	Moderately Hard to Hard Silt Clay	43	48	6	45.5	55.5	50.5	6.9	7.2	3.4	3.7	167	0.35

(continued on next page)

**Table A1 (continued)**

No.	Soil Description	Top Depth (m)	Bottom Depth (m)	Effective Unit Weight (kN/m³)	Design Shear Strength Lower Limit (kPa)	Design Shear Strength Upper Limit (kPa)	Design Shear Strength Average (kPa)	Drilling Pressure Lower Limit (kN)	Drilling Pressure Upper Limit (kN)	Flow Rate Lower Limit (m³/min)	Flow Rate Upper Limit (m³/min)	Drill Bit Extension (mm)	Bit-to-Casing Size Ratio
3	Moderately Hard to Hard Silt Clay	48	53	6	55.5	65.5	60.5	7.3	7.6	3.7	4	167	0.35
3	Moderately Hard to Hard Silt Clay	53	58	6	65.5	75.5	70.5	7.7	8	4	4.3	167	0.35
3	Moderately Hard to Hard Silt Clay	58	63	6	75.5	82	78.75	8	8.2	4.3	4.5	167	0.35
3	Moderately Hard to Hard Silt Clay	63	65	6	82	84	83	8	8.2	4.3	4.5	167	0.35
4	Hard Silt Clay	65	67.2	7	68	76	72	7.5	7.9	3.7	3.9	167	0.35
4	Hard Silt Clay	67.2	69.4	7	76	84	80	7.9	8.2	3.9	4.2	167	0.35
5	Hard Silt Clay	69.4	74.4	7	84	86.5	85.25	8.2	8.5	4.2	4.5	167	0.35
5	Hard Silt Clay	74.4	79.4	7.5	86.5	91.25	88.875	8.1	8.5	4.2	4.5	167	0.35
5	Hard Silt Clay	79.4	82.5	7.5	91.25	96	93.625	8.1	8.5	4.2	4.5	167	0.35
6	Hard to Very Hard Silt Clay	82.5	87.5	7.5	96	101	98.5	8.1	8.5	4.2	4.5	167	0.35
6	Hard to Very Hard Silt Clay	87.5	92.5	7.5	101	109	105	8.1	8.5	4.2	4.5	167	0.35
6	Hard to Very Hard Silt Clay	92.5	97.5	7.5	109	117	113	8.1	8.5	4.2	4.5	167	0.35
6	Hard to Very Hard Silt Clay	97.5	100	7.5	117	128	122.5	8.1	8.5	4.2	4.5	167	0.35

## References

- Akers, T.J., 2008. Jetting of structural casing in deepwater environments: job design and operational practices. *SPE Drill. Complet.* 23, 29–40.
- Al-Bared, M.M., Marto, A., 2017. A review on the geotechnical and engineering characteristics of marine clay and the modern methods of improvements. *Malaysian J. Fundam. Appl. Sci.* 13, 825–831.
- Al Shalabi, L., Shaaban, Z., Kasasbeh, B., 2006. Data mining: a preprocessing engine. *J. Comput. Sci.* 2, 735–739.
- Beck, R., Jackson, C., Hamilton, T., 1991. Reliable deepwater structural casing installation using controlled jetting. In: *SPE Annual Technical Conference and Exhibition*, SPE-22542-MS.
- Bedi, J., Toshniwal, D., 2018. Attribute selection based on correlation analysis. *Adv. Big data and Cloud Comp.* 51–61.
- Bienen, B., Cassidy, M., Randolph, M., Teh, K., 2010. Characterisation of undrained shear strength using statistical methods. In: *Frontiers in Offshore Geotechnics II*. CRC Press, pp. 679–684.
- Bishop, Christopher M., 1995. *Neural Networks for Pattern Recognition*. Oxford university press.
- Brevik, E.C., Calzolari, C., Miller, B.A., Pereira, P., Kabala, C., Baumgarten, A., Jordán, A., 2016. Soil mapping, classification, and pedologic modeling: history and future directions. *Geoderma* 264, 256–274.
- Changbin, K., Jin, Y., Xiaocong, Y., Chao, F., Nanding, H., Lei, L., Yuming, Y., Can, Z., Huanhuan, W., Fatai, A., 2018. Bearing characteristics of composite conductor structure: deepwater conductor pipe with Suction Bucket foundation. In: *Offshore Technology Conference Asia*. OTC.
- Chen, D., Wang, Y., Gao, W., 2020. Combining a gradient-based method and an evolution strategy for multi-objective reinforcement learning. *Appl. Intell.* 50, 3301–3317.
- Friedman, E., Fontaine, F., 2018. Generalizing across multi-objective reward functions in deep reinforcement learning arXiv preprint arXiv:1809.06364.
- Geelen, C., Yntema, D., Jaap, M., Keesman, K., 2021. Optimal sensor placement in hydraulic conduit networks: a state-space approach. *Water* 13, 3105, 2021.
- Hausknecht, M., Stone, P., 2015. Deep reinforcement learning in parameterized action space arXiv preprint arXiv:1511.04143.
- Hribar, J., Hackett, L., Dusparic, I., 2022. Deep W-Networks: Solving Multi-Objective Optimisation Problems with Deep Reinforcement Learning arXiv preprint arXiv: 2211.04813.
- Jeanjean, P., 2002. Innovative design method for deepwater surface casings. In: *SPE Annual Technical Conference and Exhibition?*, SPE-77357-MS.
- Joseph, V.R., 2022. Optimal ratio for data splitting. *Stat. Anal. Data Min.: The ASA Data Sci. J.* 15, 531–538.
- Kan, C., Gao, D., Yang, J., 2020. Experimental study on critical displacement for drill-conductor injection during deepwater drilling. *SPE J.* 25, 2206–2219.
- Kan, C., Yang, J., Yu, X., Meng, W., Hu, N., Zhou, B., Zhang, B., Hu, Z., 2016. Numerical simulation of thermal stress on entrapped pressure of deepwater and further research on anti-thermal-stress casing tools. In: *SPE/AAPG Africa Energy and Technology Conference*. OnePetro.
- Kim, S., Kim, I., You, D., 2022. Multi-condition multi-objective optimization using deep reinforcement learning. *J. Comput. Phys.* 462, 111263.
- King, G.W., Solomon, I.J., 1995. The instrumentation of the conductor of a subsea well in the North Sea to measure the installed conditions and behavior under load. *SPE Drill. Complet.* 10, 265–270.
- Kuhn, M., Johnson, K., 2013. *Applied Predictive Modeling*. Springer.
- Lee, B.K., Jeong, J.S., Fan, L.G., Jin, T.K., 1999. Free vibrations of tapered piles embedded partially in Winkler type foundations. *KSCE J. Civ. Eng.* 3, 195–203.
- Li, K., Zhang, T., Wang, R., 2020. Deep reinforcement learning for multiobjective optimization. *IEEE Trans. Cybern.* 51, 3103–3114.
- Liu, J., Lin, Y., Yang, J., Yin, Q., 2022. A robust and efficient method to geometrically calculate the minimum bit stick-out in a deepwater conductor jetting project. *J. Petrol. Sci. Eng.* 208, 109620.
- Lorenzo, P.R., Nalepa, J., Kawulok, M., Ramos, L.S., Pastor, J.R., 2017. Particle swarm optimization for hyper-parameter selection in deep neural networks. In: *Proceedings of the Genetic and Evolutionary Computation Conference*, pp. 481–488.
- Mbarak, W.K., Cinicioğlu, E.N., Cinicioğlu, O., 2020. SPT based determination of undrained shear strength: regression models and machine learning. *Front. Struct. Civ. Eng.* 14, 185–198.
- Ngatchou, P., Zarei, A., El-Sharkawi, A., 2005. Pareto multi objective optimization. In: *Proceedings of the 13th International Conference on Intelligent Systems Application to Power Systems*, pp. 84–91.

- Park, S., Kwak, N., 2017. Analysis on the dropout effect in convolutional neural networks. In: Computer Vision–ACCV 2016: 13th Asian Conference on Computer Vision, Taipei, Taiwan, November 20–24, 2016, Revised Selected Papers, Part II 13. Springer, pp. 189–204.
- Petchrompo, S., Coit, D.W., Brintrup, A., Wannakrairot, A., Parlakad, A.K., 2022. A review of Pareto pruning methods for multi-objective optimization. *Comput. Ind. Eng.* 167, 108022.
- Plappert, M., Houthooft, R., Dhariwal, P., Sidor, S., Chen, R.Y., Chen, X., Asfour, T., Abbeel, P., Andrychowicz, M., 2017. Parameter Space Noise for Exploration arXiv preprint arXiv:1706.01905.
- Ruchite, M., Grabocka, J., 2021. Scalable pareto front approximation for deep multi-objective learning. In: 2021 IEEE International Conference on Data Mining (ICDM), pp. 1306–1311.
- Schaal, T., Quan, J., Antonoglou, I., Silver, D., 2015. Prioritized Experience Replay arXiv preprint arXiv:1511.05952.
- Siddiqui, F., Sargent, P., Montague, G., 2020. The use of PCA and signal processing techniques for processing time-based construction settlement data of road embankments. *Adv. Eng. Inf.* 46, 101181.
- Tani, L., Rand, D., Veelken, C., Kadastik, M., 2021. Evolutionary algorithms for hyperparameter optimization in machine learning for application in high energy physics. *The European Phys. J.* 81, 1–9.
- Turkson, P., VandenBerge, D.R., 2023. Statistical analysis of undrained strength as linear function of depth. *GeoCongress* 62–71.
- Wang, T., Song, B., 2019. Study on deepwater conductor jet excavation mechanism in cohesive soil. *Appl. Ocean Res.* 82, 225–235.
- Wang, T., Sun, B.J., 2008. Lateral bearing capacity of jetting structural casing of wellhead in deepwater. *J. China Univ. Petroleum* 5, 50–53.
- Wang, Y.y., Chen, Z.h., Yan, Q., Hu, Y.d., Wang, C., Luo, W.t., Cai, B.p., 2022. A dynamic failure analysis methodology for fault diagnosis of fatigue cracks of subsea wellhead connectors with material aging. *Process Saf. Environ. Protect.* 159, 36–52.
- Wang, Y., Zhang, W., Qi, X., Ching, J., 2022. Data analytics in geotechnical and geological engineering. *Georisk* 16, 1, 1.
- Xu, Y., Guan, Z., Su, K., 2014. Methods of setting depth range with credibility of conductor for deepwater drilling based on probability statistics. *Appl. Ocean Res.* 48, 301–307.
- Yang, C., Yang, G., Zhang, J., Ma, H., 2019. Analysis technics of seismic signals. In: Three Dimensional Space-Time Analysis Theory of Geotechnical Seismic Engineering. Springer Singapore, Singapore, pp. 31–63.
- Yang, F., Huang, H., Shi, W., Ma, Y., Feng, Y., Cheng, G., Liu, Z., 2023. PMDRL: pareto-front-based multi-objective deep reinforcement learning. *J. Ambient Intell. Hum. Comput.* 14, 12663–12672.
- Yang, J., 2023. Jetting installation method of oil-gas well conductor. In: Installation Methods of Offshore Oil-Gas Well Conductor. Springer Nature Singapore, Singapore, pp. 107–162.
- Ye, F., 2017. Particle swarm optimization-based automatic parameter selection for deep neural networks and its applications in large-scale and high-dimensional data. *PLoS One* 12, e0188746.
- Zhao, X., Yin, Q., Yang, J., Long, Y., Liu, H., Guo, Y., 2022. Risk assessment of surface conductor jetting installation during deep-water drilling in sloping seabed. *Ocean Eng.* 266, 113057.
- Zhou, B., Yang, J., Liu, Z., Zhou, R., 2016. Model and experimental study on jetting flow rate for installing surface conductor in deep-water. *Appl. Ocean Res.* 60, 155–163.
- Zhu, J., Wu, F., Zhao, J., 2021. An overview of the action space for deep reinforcement learning. In: Proceedings of the 2021 4th International Conference on Algorithms, Computing and Artificial Intelligence, pp. 1–10.